MODELING SHAPE DISTORTION OF 3-D PRINTED ALUMINUM OXIDE PARTS DURING SINTERING

by

Nicholas Cox

B.S. in Mechanical Engineering, University of Pittsburgh, 2018

Submitted to the Graduate Faculty of

Swanson School of Engineering in partial fulfillment

of the requirements for the degree of

Master of Science in Mechanical Engineering

University of Pittsburgh

2018

UNIVERSITY OF PITTSBURGH

SWANSON SCHOOL OF ENGINEERING

This thesis was presented

by

Nicholas Cox

It was defended on

January 10, 2018

and approved by

Ian Nettleship, Ph.D., Associate Professor

Department of Mechanical Engineering and Materials Science

William Slaughter, Ph.D., Associate Professor

Department of Mechanical Engineering and Materials Science

Thesis Advisor: David Schmidt, Ph.D., Assistant Professor

Department of Mechanical Engineering and Materials Science

MODELING SHAPE DISTORTION OF 3-D PRINTED ALUMINUM OXIDE PARTS DURING SINTERING

Nicholas Cox, M.S

University of Pittsburgh, 2018

Ceramics are often admired for their unique mechanical properties, such as high melting temperature, and low thermal conductivity. They have a wide array of industrial applications from the aerospace to automotive industry. However, ceramics can often be overlooked in some applications because of their difficult and expensive manufacturability. To resolve this issue, 3-D printing has become a growing method of manufacturing ceramic parts more efficiently, and an increasingly researched topic. 3-D printing often results in inhomogeneous low-density parts that are often inadequate for many mechanical applications. To effectively manufacture a 3-D printed ceramic part, it is essential to apply a heat treatment, sintering, to the part to achieve an increased density. Often, the density changes during sintering are non-uniform and may create unwanted shape distortions. This thesis aims to investigate the prediction of shape changes within aluminum oxide parts throughout sintering. This would allow engineers to design parts to a desired dimension, without having to correct for shape distortion using iterative process. To this

end, a constitutive relationship tailored for the sintering of aluminum oxide was developed. A literature review was conducted to determine the best form of the constitutive relationship, and several material parameters were determined. The form identified was implemented as a user defined constitutive relationship inside the commercial finite element software Abaqus. Using this model trends associated with sintering behavior of aluminum oxide were identified.

TABLE OF CONTENTS

LIST OF TABLES

LIST OF FIGURES

ACKNOWLEDGEMENTS

First, I would like to express my extreme thanks and gratitude to Dr. David Schmidt. Without his patience, guidance, and support throughout my graduate career, this work would have never been possible. Next, I would like to thank Dr. Ian Nettleship and Dr. William Slaughter for their insight and knowledge on this project. I would, also, like to thank my fiancé, Casey Smith, for her support and encouragement throughout my graduate studies. I would like to thank my parents, Timothy and Elizabeth Cox, for always pushing me to strive for excellence. Last I want to thank my family and friends for their constant support.

1.0 INTRODUCTION

Ceramic parts have become increasingly valuable in many different engineering applications due to their high melting point and other desirable mechanical properties. When manufacturing ceramic parts with complicated geometries, 3-D printing has become a very useful production method. When creating 3-D printed ceramic parts, producing the desired properties are based on achieving the proper microstructure. After printing, the density of the part is low and the resulting microstructure is inadequate for many engineering applications. To increase the density of the part, and create the desired mechanical properties the part must be heat treated. This process is known as sintering. Sintering entails heating a part, which has already been formed, so that densification occurs [1]. During the sintering process, distortion and non-uniform densification occurs. This is a result of non-uniform pore distribution throughout the material resulting in inhomogeneous material density. Friction upon shrinkage and gravity also play roles in the non-uniform sintering [2]. The prediction of non-uniform densification and distortion of the manufactured part is essential to efficiently manufacture ceramic parts to a predetermined dimension. The objective of this thesis is to generate techniques for modeling 3-D printed ceramics (Aluminum Oxide) during the sintering process to accurately predict shrinkage and distortion. A continuum mechanics approach was taken to create a constitutive model that describes the relationship between the stress and strain tensor during the sintering process. The

constitutive model was utilized in creating a user subroutine (UMAT) to implement into the FEA program, Abaqus.

2.0 LITERATURE REVIEW AND BACKGROUND

This section introduces the basic concepts of the sintering process as well as the background used to develop a UMAT in Abaqus. The background of the general sintering process is explained, and specific continuum models are introduced. The material parameters that were determined for aluminum oxide sintering are also discussed.

2.1 SINTERING PROCESS

2.1.1 Introduction

Sintering is a heat treatment process in which heat, and sometimes pressure, is applied to a porous body to induce densification. There are many factors that affect the microstructure produced by sintering, such as the sintering temperature, time, and the temperature distribution. Sintering, with the addition of pressure, is sometimes required to achieve higher densities that are needed for specific microstructures, but have drawbacks such as high fabrication costs. Sintering is driven by the reduction in surface free energy of the system due to the pores within the compact. This can be dependent on the curvature of the particles in the compact, as well as the specific energy [1].

2.1.2 Categories of sintering

Sintering can be divided into four categories. The categories are dependent upon the way the material behaves, and the material properties desired. These are solid-state, liquid, vitrification, and viscous sintering [1].

- Solid State: Solid State is the sintering process in which the porous material is heated to approximately 50 to 90 percent of the melting temperature. Densification is driven by atomic diffusion.
- Liquid phase: Liquid phase sintering includes a small amount of additive present with the solid matrix of material. This additive becomes a liquid at sintering temperatures. The liquid is used as an aid to enhance the densification of the solid matrix.
- Vitrification: This process also includes an additive present, but a much larger amount (25% of solid volume). This additive fills the remaining pores in the solid matrix through fluid flow upon heating.
- Viscous: This process is characterized by heating glass particles close to the softening temperature, and the glass flows due to surface tension between the particles.

2.1.3 Transport mechanisms

There are six mass transport mechanisms in which sintering can occur in crystalline materials. There are three mechanisms which do not alter the material's density but only alter the microstructure of the material. These are surface diffusion, lattice diffusion, and vapor transport. The other three mechanisms increase the density of the material; decreasing the volume of the material due to shrinkage [1]. The mechanisms of sintering are described in figure 1 below.

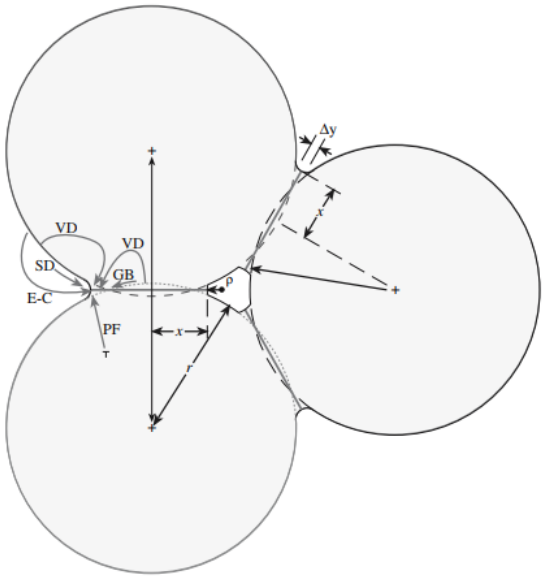

Figure 1. Sintering diffusion paths [3]

Table 1 Sintering Mechanisms and Transport [3]			
Mechanism	Transport Path		Source
SD	Surface Diffusion		Surface
VD	Volume Diffusion		Surface
E-C	Evaporation-Condensation		Surface
GB	Grain Boundary diffusion		GB
VD	Volume Diffusion		GB
PF	Plastic Flow		Dislocations

2.1.4 Stages of sintering

During sintering, the material's microstructural changes can be described in stages, including the initial, intermediate, and final stages. These stages are separated by densification, particle interaction, and grain growth. Grain growth occurs when the high temperature during sintering

causes smaller grains to shrink and larger grains to grow due to the nature of their curvature. The stages of sintering are shown in figure 2 below.

- Initial (II): During the initial stage densification is low at approximately 5 percent. This stage is characterized by “atomic mobility” where the contacting particles start to form necks.
- Intermediate (III): The intermediate stage has large increases in densification to approximately 90 to 95% of full density. The large areas of pores are consolidated into channels surrounded by particles. In this stage, grain growth becomes a contributing factor.
- Final (IV): The final stage is when the channels of porosity close off into individual pores. At this point, the party is only a few percent from being fully dense [3].

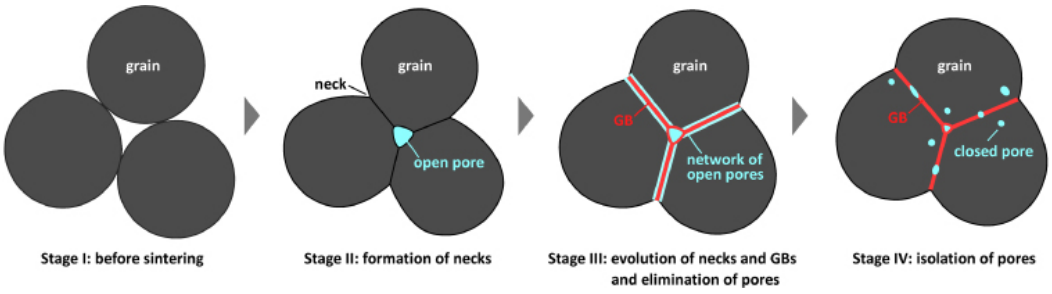

Figure 2. Stages of sintering [4]

2.2 CONTINUUM APPROACH

To describe the mechanical response of aluminum oxide during sintering, a continuum mechanics analysis was adopted. This would allow a macroscopic description of the shape distortions and density changes throughout the sintering process. A continuum based constitutive model allowed for the development of a user material subroutine to be implemented into Abaqus.

2.2.1 Introduction

The continuum formulation of sintering describes the material as having two phases present, the solid body or “skeleton” and the voids or “Pores.” The pores are assumed to be homogeneously distributed throughout the skeleton. Figure 3 shows a visual representation of the continuum formulation of a sintering body [11].

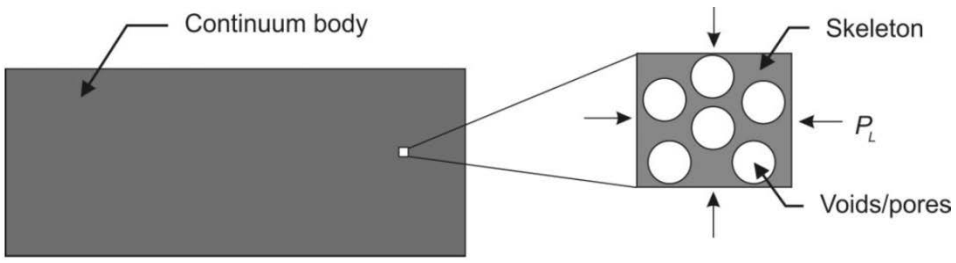

Figure 3. Sintering body [11]

The skeleton can be assumed to be incompressible linear-viscous, incompressible nonlinear-viscous, or compressible nonlinear-viscous [5]. For the purposes of this thesis, the skeleton was assumed to be linear-viscous. The driving force that induces densification of the part is due to the capillary stresses between the particles [7]. Often, external pressure is applied to aid in

densification, but for the purposes of this thesis, free sintering (no external pressure) is considered.

2.2.2 Adopted constitutive approach

The constitutive model utilized in this thesis is one developed by Olevsky [5]. The general form of the constitutive equation is given by equation (1) below. The terms in equation (1) are given in table 2.

$$\sigma_{ij} = \frac{\sigma(W)}{W}\left(\varphi\dot{\varepsilon}_{ij}{}' + \psi\dot{e}\delta_{ij}\right) + P_L\delta_{ij} \quad (1)$$

Table 2. Constitutive Model Parameters [5]

Parameter	***Symbol***
Cauchy stress tensor	σ_{ij}
Equivalent stress	$\sigma(W)$
Equivalent strain rate	W
Deviatoric strain rate tensor	$\dot{\varepsilon}_{ij}{}'$
Trace of strain rate tensor	$\dot{e}$
Normalized shear viscosity	φ
Normalized bulk viscosity	ψ
Sintering stress	P_L
Kronecker delta	δ_{ij}

For the linear viscous case, the equivalent stress is represented as $\sigma(W) = 2\eta_0 W$, where η_0 is the initial shear viscosity of the solid body. This gives the linear viscous form of the constitutive equation given by equation (2).

$$\sigma_{ij} = 2\eta_0\left(\varphi\dot{\varepsilon}_{ij}{}' + \psi e\delta_{ij}\right) + P_L\delta_{ij} \quad (2)$$

It is useful to invert the stress form of the constitutive relationship and express the normalized shear and bulk viscosities in terms of effective shear and bulk viscosities. The inverted equation represents the inelastic portion of the strain rate. This is given in equation (3) below [6].

$$\dot{\varepsilon}_{ij} = \frac{\sigma'_{ij}}{2G_{SOVS}} + \frac{(\sigma_m - \sigma_{SOVS})}{3K_{SOVS}}\delta_{ij} \tag{3}$$

Where σ_m is the hydrostatic stress, σ'_{ij} is the deviatoric stress tensor, and the effective viscosities are related to the normalized viscosities by equations (4) and (5).

$$G_{SOVS} = \eta_o \varphi \tag{4}$$

$$K_{SOVS} = \eta_o \psi \tag{5}$$

Olevsky proposed simplified forms of the normalized viscosities and sintering stress. The bulk and shear viscosities as well as the sintering stress forms are given in equations (6-8) below.

$$G_{SOVS} = \eta_o (1-\theta)^2 \tag{6}$$

$$K_{SOVS} = \eta_o \frac{4(1-\theta)^3}{3\theta} \tag{7}$$

$$\sigma_{SOVS} = \frac{3\gamma}{r_0}(1-\theta)^2 \tag{8}$$

Where γ is the surface tension between particles, θ is the ratio of pore volume to the total volume, and r_0 is the initial powder particle radius [5]. These make for simple expressions, but are lacking accuracy with experimental data. The accuracy of the model is predominantly

dependent on the forms of the viscosities and sintering stress. There have been studies conducted to identify more detailed forms of the moduli to increase predictability of the model. A modified version of the Olevsky model was proposed to better match experimental results.

2.2.2.1 Implemented constitutive model

Although the model developed by Olevsky is suitable for implementation into FEA software, there are shortcomings in correlation with experimental results. Also, grain growth during the sintering process is never addressed in the model. To create a more accurate constitutive model a grain growth factor was added and the viscosity is expressed as an Arrhenius type function. The modified implemented model is given by equation (9) below. These changes provide a more accurate description of the solidification of aluminum oxide during sintering [6].

$$\dot{\varepsilon}_{ij} = \frac{1}{2\eta}\frac{1}{\rho^{2n-1}}\left[\sigma'_{ij} + \frac{2}{9{f_s}^2}(\sigma_m - \sigma_{SOVS})\delta_{ij}\right] \tag{9}$$

The constants for equation (9) have been taken from the literature and are given in Table 3.

Table 3. Modified SOVS aluminum oxide material parameters [6]

Parameter	***Symbol***	***Value***	***Unit***
Viscosity Constants	C_{s1}	7.82e15	[-]
	C_{s2}	3.23e4	[-]
Exponential constant for bulk and shear viscosities	n	2.5	[-]
Sintering stress exponential constant	N_s	5.0	[-]
Sintering stress correction factor	ξ	0.5	[-]
Specific surface energy	γ	0.9	$[\frac{J}{m^2}]$
Grain evolution exponent	m	1/0.37	[-]
Grain evolution coefficient	β	4.84e-20	[-]
Grain radius	R	-	[m]

2.2.2.2 Model parameterization

The normalized shear and bulk viscosities as well as the sintering stress are functions of temperature and relative density. The forms of these parameters differ for different materials and their accuracy are important to the overall accuracy of the model. One way of determining these expressions is through empirical data. This is done by curve fitting onto data taken from sintering experiments. In the case of aluminum oxide, the forms of the viscosity functions are functions of the shear viscosity of the fully dense skeleton material.

The shear viscosity of the fully dense skeleton describes the flow of the material as a result of the capillary stresses (sintering stress) between the particles. Reiterer and Ewsuk proposed a form of the shear viscosity for ceramics when grain boundary diffusion is the rate controlled material flow mechanism that results in inelastic deformation. They suggested that an Arrhenius-Type viscosity function can be used to describe the material flow during sintering [9]. The shear viscosity of the fully dense skeleton is given in equation (10).

$$\eta_o = C_{s1} T exp\left(\frac{C_{s2}}{T}\right) d^3 \tag{10}$$

C_{s1}, and C_{s2} are constants that were determined by curve fitting data from sintering experiments, and d is the grain growth factor [13]. A curve showing the agreeance between the experimental data and the curve fit function is shown in figure 4 [8]. It should be noted that figure 4 was taken from reference 8 as developed by cannon et al. It was found that there appears to be a typographical error in the constant (C_{s1}), where the exponent should be to the 15^{th} power not the 17^{th} power. Examination in context and in application validates this change.

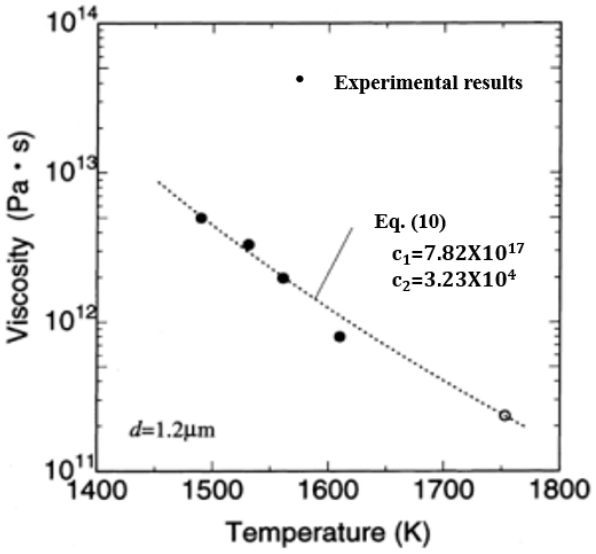

Figure 4. Shear viscosity curve comparing the proposed form to experimental results [8]

The grain growth factor is given by equation (11) [6].

$$d^m = d_0^m + \beta T \tag{11}$$

By equating equations (3) and (9), the effective shear and bulk viscosities take the form given in equations (12) and (13).

$$G_{SOVS} = \eta_o \rho^{2n-1} \tag{12}$$

$$K_{SOVS} = 3{f_s}^2 \eta_o \rho^{2n-1} \tag{13}$$

Where $f_s(\rho) = \frac{1}{2.5\sqrt{1-\rho}}$ and the sintering stress are functions of relative density. The sintering stress is shown in equation (14).

$$\sigma_s = \frac{2\gamma}{\xi R}\rho^{N_s}\left[\frac{\rho(1-\rho_0)}{\rho_0(1-\rho)}\right]^{\frac{1}{3}} \quad (14)$$

ρ is the relative density, and ρ_0 is the initial green density. The constant values were taken from the literature and are given in table 3 [6].

2.2.2.3 Adopted density evolution

During densification, shrinkage of the part occurs resulting in a lower overall volume but higher density. If the mass of the air present in the pores is ignored, mass must be conserved during this process. This results in an expression for the rate change in volume given by equation (15) [5].

$$\dot{\rho} = -\rho \cdot \dot{e} \quad (15)$$

Where $\dot{e}$ is the trace of the strain rate tensor and takes the form given in equation (16).

$$\dot{e} = tr(\dot{\varepsilon}) = \dot{\varepsilon}_{kk} = \frac{d(\varepsilon_{kk})}{dt} \quad (16)$$

Taking the rate form of equation (15) gives equation (17).

$$\frac{d\rho}{dt} = -\rho\frac{d(\varepsilon_{kk})}{dt} \quad (17)$$

Integration of equation (17) yields equation (18).

$$\rho(\varepsilon) = Cexp^{(-\varepsilon_{kk})} \quad (18)$$

Applying initial conditions gives equation (19) which describes the density as a function of strain.

$$\rho(\varepsilon) = \rho_0 exp^{(-\varepsilon_{kk})} \tag{19}$$

Where ρ_0 is the initial density of the part.

2.3 CONSTITUTIVE MODEL DEVELOPMENT

2.3.1 Introduction

Abaqus is a commercially available finite element based software package that is used for simulations that range from static to thermal. Within Abaqus, user material subroutines (UMAT) can be used to describe a material's behavior. A UMAT is used when the needed material response is not available within the standard constitutive models offered by Abaqus. This makes it possible to create models that replicate complicated material behavior that would not normally be able to be simulated using the standard Abaqus software.

2.3.2 Model framework

There are two main tasks that the UMAT must complete when running a simulation. These functions are updating the incremental stress, and returning the Jacobian matrix of the constitutive model. In order to do this, Abaqus must be able to calculate a strain tensor based on

the relationship between stress and strain defined in the constitutive model. Other parameters, such as incremental change in time and temperature are calculated by the software and passed to the UMAT from Abaqus [14].

2.3.2.1 Constitutive model

Abaqus requires the UMAT to define the Cauchy stress and appropriate Jacobian at each time increment. The incremental form of the stress tensor is formulated using the assumption that elastic strain can be ignored. This assumption is reasonable, as elastic strain is very small in pressureless sintering. With this assumption, the stress is derived from the visco-plastic strain and takes the form of equation (20) [10].

$$\sigma = 2G_p\dot{\varepsilon}_{vp} + \left(K_p - \frac{2}{3}G_p\right)\dot{e}_{vp}I + \sigma_s I \tag{20}$$

The incremental form of the stress tensor was found using the central difference method described in equations (21) and (22).

$$\dot{f}_{t+\frac{1}{2}t} = \frac{\Delta f}{\Delta t} \tag{21}$$

$$f_{t+\frac{1}{2}t} = f_t + \frac{\Delta f}{2} \tag{22}$$

Where f is the function, f_t is the function evaluated at the beginning of the time increment, Δf is the change in the fuction over the time increment, and Δt is the increment in time. Using the central difference method, equation (20) is expressed in its incremental form given in equation (23).

$$\sigma_t + \frac{\Delta\sigma}{2} = 2G_p \frac{\Delta\varepsilon}{\Delta t} + \left(K_p - \frac{2}{3}G_p\right)\frac{\Delta e_{vp}}{\Delta t} I + \sigma_s I \tag{23}$$

This yields the change in stress at the end of the increment given in equation (24).

$$\Delta\sigma = 4G_p \frac{\Delta\varepsilon}{\Delta t} + \left(2K_p - \frac{4}{3}G_p\right)\frac{\Delta e_{vp}}{\Delta t} I + 2\sigma_s I - 2\sigma_t \tag{24}$$

The scalar components of equation (24) in indicial notation is given by equation (25)

$$\Delta\sigma_{ij} = 4G_p \frac{\Delta\varepsilon_{ij}}{\Delta t} + \left(2K_p - \frac{4}{3}G_p\right)\frac{\Delta\varepsilon_{kk}}{\Delta t}\delta_{ij} + 2\sigma_s\delta_{ij} - 2\sigma_{t_{ij}} \tag{25}$$

The stress that must be updated at the end of each increment is defined as the stress at the beginning of the increment plus the change in stress over the increment. This expression is given in equation (26) [10].

$$\Delta\sigma + \sigma_t = 4G_p \frac{\Delta\varepsilon}{\Delta t} + \left(2K_p - \frac{4}{3}G_p\right)\frac{\Delta e_{vp}}{\Delta t} I + 2\sigma_s I - \sigma_t \tag{26}$$

This equation was coded into the material subroutine to update the stress at the end of each increment.

2.3.2.2 Jacobian

For the simulation to come to rapid convergence, an accurate definition of the Jacobian matrix of the constitutive model must be formulated. The Jacobian, or tangent matrix, relates the change in stress or stress rate to the change in strain or strain rate. The Jacobian is defined as $\frac{\partial \Delta\sigma}{\partial \Delta\varepsilon}$ and must be updated at the end of each increment, as its components are dependent on the current temperature, time step etc. The Jacobian is calculated by differentiating the incremental stress equation (24) with respect to the change in incremental strain [10]. The Jacobian matrix takes the form in equation (26) below [12].

$$\frac{\partial \Delta\sigma}{\partial \Delta\varepsilon} = \begin{bmatrix} \frac{\partial \Delta\sigma_{11}}{\partial \Delta\varepsilon_{11}} & \frac{\partial \Delta\sigma_{11}}{\partial \Delta\varepsilon_{22}} & \frac{\partial \Delta\sigma_{11}}{\partial \Delta\varepsilon_{33}} & \frac{\partial \Delta\sigma_{11}}{\partial \Delta\varepsilon_{12}} & \frac{\partial \Delta\sigma_{11}}{\partial \Delta\varepsilon_{23}} & \frac{\partial \Delta\sigma_{11}}{\partial \Delta\varepsilon_{31}} \\ \frac{\partial \Delta\sigma_{22}}{\partial \Delta\varepsilon_{11}} & \frac{\partial \Delta\sigma_{22}}{\partial \Delta\varepsilon_{22}} & \frac{\partial \Delta\sigma_{22}}{\partial \Delta\varepsilon_{33}} & \frac{\partial \Delta\sigma_{22}}{\partial \Delta\varepsilon_{12}} & \frac{\partial \Delta\sigma_{22}}{\partial \Delta\varepsilon_{23}} & \frac{\partial \Delta\sigma_{22}}{\partial \Delta\varepsilon_{31}} \\ \frac{\partial \Delta\sigma_{33}}{\partial \Delta\varepsilon_{11}} & \frac{\partial \Delta\sigma_{33}}{\partial \Delta\varepsilon_{22}} & \frac{\partial \Delta\sigma_{33}}{\partial \Delta\varepsilon_{33}} & \frac{\partial \Delta\sigma_{33}}{\partial \Delta\varepsilon_{12}} & \frac{\partial \Delta\sigma_{33}}{\partial \Delta\varepsilon_{23}} & \frac{\partial \Delta\sigma_{33}}{\partial \Delta\varepsilon_{31}} \\ \frac{\partial \Delta\sigma_{12}}{\partial \Delta\varepsilon_{11}} & \frac{\partial \Delta\sigma_{12}}{\partial \Delta\varepsilon_{22}} & \frac{\partial \Delta\sigma_{12}}{\partial \Delta\varepsilon_{33}} & \frac{\partial \Delta\sigma_{12}}{\partial \Delta\varepsilon_{12}} & \frac{\partial \Delta\sigma_{12}}{\partial \Delta\varepsilon_{23}} & \frac{\partial \Delta\sigma_{12}}{\partial \Delta\varepsilon_{31}} \\ \frac{\partial \Delta\sigma_{23}}{\partial \Delta\varepsilon_{11}} & \frac{\partial \Delta\sigma_{23}}{\partial \Delta\varepsilon_{22}} & \frac{\partial \Delta\sigma_{23}}{\partial \Delta\varepsilon_{33}} & \frac{\partial \Delta\sigma_{23}}{\partial \Delta\varepsilon_{12}} & \frac{\partial \Delta\sigma_{23}}{\partial \Delta\varepsilon_{23}} & \frac{\partial \Delta\sigma_{23}}{\partial \Delta\varepsilon_{31}} \\ \frac{\partial \Delta\sigma_{31}}{\partial \Delta\varepsilon_{11}} & \frac{\partial \Delta\sigma_{31}}{\partial \Delta\varepsilon_{22}} & \frac{\partial \Delta\sigma_{31}}{\partial \Delta\varepsilon_{33}} & \frac{\partial \Delta\sigma_{31}}{\partial \Delta\varepsilon_{12}} & \frac{\partial \Delta\sigma_{31}}{\partial \Delta\varepsilon_{23}} & \frac{\partial \Delta\sigma_{31}}{\partial \Delta\varepsilon_{31}} \end{bmatrix} \tag{26}$$

The first term in the Jacobian matrix is given in equation (27).

$$\frac{\partial \Delta\sigma_{11}}{\partial \Delta\varepsilon_{11}} = \left(\frac{4G_p}{\Delta t} \cdot \frac{\partial(\Delta\varepsilon_{11})}{\partial \Delta\varepsilon_{11}} + \frac{\left(2K_p - \frac{4}{3}G_p\right)}{\Delta t} \cdot \frac{\partial(\Delta e_{vp})}{\partial \Delta\varepsilon_{11}} \right) = \frac{\left(2K_p - \frac{4}{3}G_p\right)}{\Delta t} + \frac{4G_p}{\Delta t} \tag{27}$$

For simplification, the first term in equation (27) will be defined as $\left(a = \frac{\left(2K_p - \frac{4}{3}G_p\right)}{\Delta t}\right)$ and the second term as $\left(b = \frac{4G_p}{\Delta t}\right)$. Using this method, each of the scalar components of the Jacobian matrix can be determined. Using the simplified terms the Jacobian matrix is given in equation (28). For a complete derivation, see appendix A.

$$\frac{\partial \Delta\sigma}{\partial \Delta\varepsilon} = \begin{bmatrix} b+a & a & a & 0 & 0 & 0 \\ a & b+a & a & 0 & 0 & 0 \\ a & a & b+a & 0 & 0 & 0 \\ 0 & 0 & 0 & b & 0 & 0 \\ 0 & 0 & 0 & 0 & b & 0 \\ 0 & 0 & 0 & 0 & 0 & b \end{bmatrix} \tag{28}$$

2.3.2.3 Solution dependent state variables

Another function of the UMAT is to update solution dependent state variables. State variables are variables that are dependent on values that are updated each time the UMAT is called. These values could be calculated in the UMAT, or values that are updated by Abaqus and passed back to the UMAT [14]. In this simulation, the state variables are the sintering stress σ_s , $f_s(\rho)$, the shear viscosity η_o, and the density $\rho(\varepsilon)$.

3.0 MODEL VERIFICATION

The strategy used to verify the model was to compare results presented in Van et al [6]. In this reference there are two cases to that were used to validate the accuracy of the model. The two validation cases were recreated using the developed UMAT. These cases were, then, compared to the results found in the literature.

3.1 CYLINDER

3.1.1 Model process parameters

The first validation case that was conducted was a cylinder with pressure of 20 Mpa applied to the top face of the cylinder. The initial grain radius was 0.15 microns, with an initial green density of 0.59 that was homogenous throughout the part. The cylinder is 8.9 mm in diameter, and 10.38 mm tall. For simplicity, the simulation was conducted using a 2D axisymmetric case. This was done because the intention of this case was just to determine the validity of the constitutive model. A schematic of one half of the axisymmetric geometry is given in figure 5, and the temperature profile is shown in figure 6.

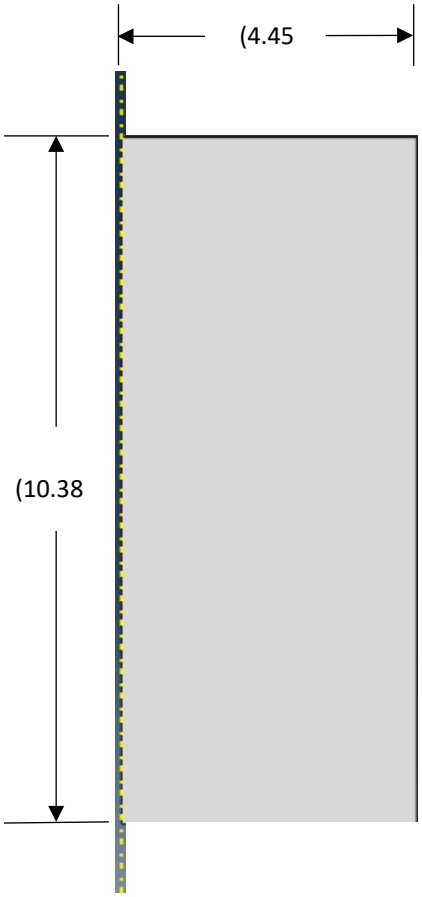

Figure 5. Half cylinder (axisymmetric) geometry for validation trial

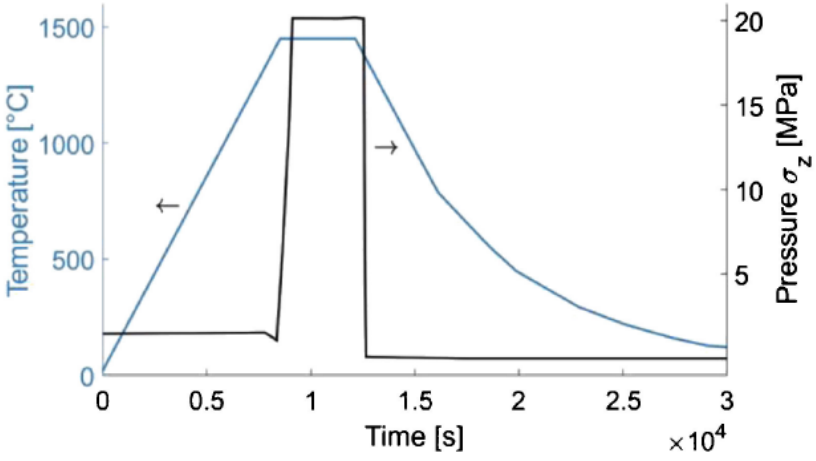

Figure 6. Cylinder temperature profile for validation trial [6]

3.1.2 Results

The results from the cylinder sintering trial are discussed in this section. Figure 7 shows the magnitude of the final deformation after pressure assisted sintering. The overlay shows the geometry of the cylinder before the simulation, and the contour plot shows the figure after deformation. The expected geometrical change was a barrel shape as the pressure on the top surface compresses the part. This shape change is the result of the processing characteristics illustrated in figure 7.

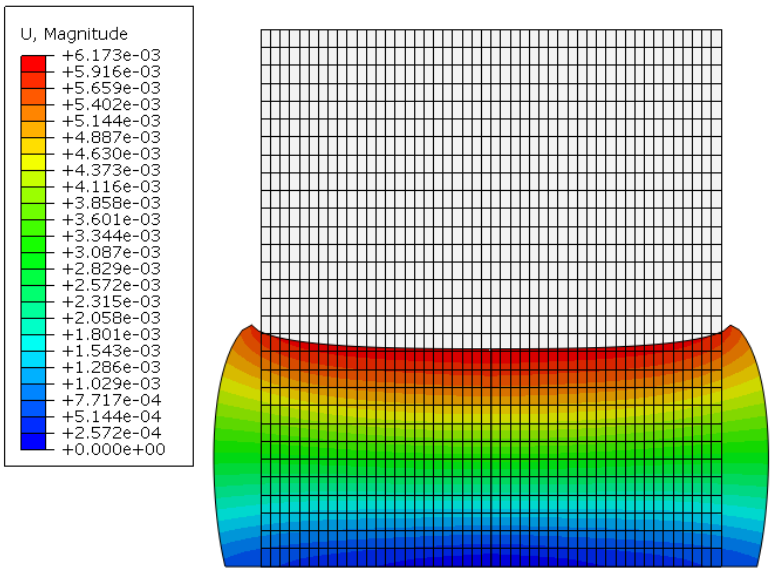

Figure 7. Magnitude of final deformation after pressure assisted sintering. Contours indicate the deformation sum. Overlay illustrates the initial geometry and associated finite element mesh.

Figure 8 shows the displacement response of a cylinder undergoing a pressure-assisted sintering as presented by Van et al [6]. This shows reasonable agreement, in terms of deformation pattern and magnitude, with the simulated response presented in figure 7. A quantitative comparison could not be made as the analysis presented by Van et al [6] did not document the specific deformation magnitude.

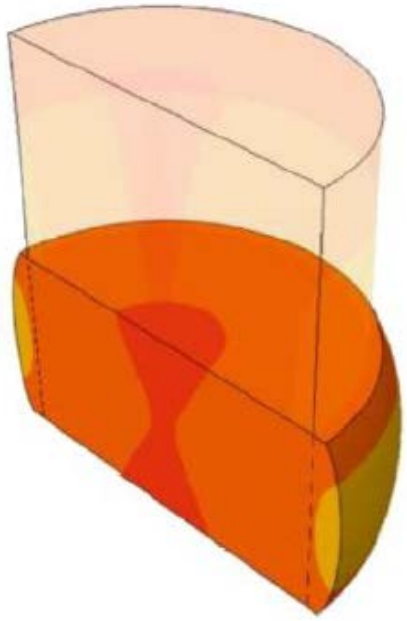

Figure 8. Simulated response to pressure-assisted sintering of a cylinder with uniform initial density presented Van et al [6]

The evolution of density, associated with the verification model, is summarized in Figures 9 through 12. The first plot, figure 9, shows the initial uniform density throughout the part. The Abaqus UMAT framework allows for the definition of user specific state variables. In the model state variable 4 (SDV4) is defined as the density for each time increment.

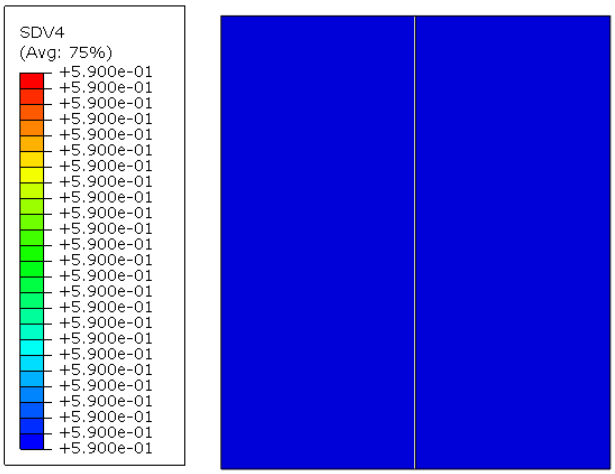

Figure 9. Initial geometry of axisymmetric model. Contour overlay illustrates initial uniform density of 59 percent associated with the green compact.

As the simulation evolved, the density is changing more rapidly in the center of the cylinder. This is driven by the variation in strain throughout the compact; regions associated with larger strain magnitudes experience a greater densification rate. This behavior leads to the resulting barrel shape shown in figure 7.

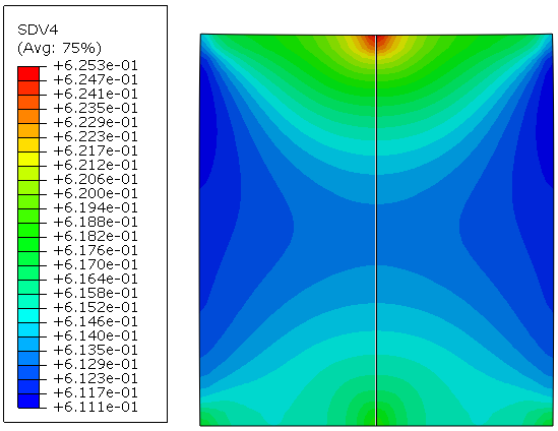

Figure 10. Variation in densification magnitude within the compact at 10% of sintering time.

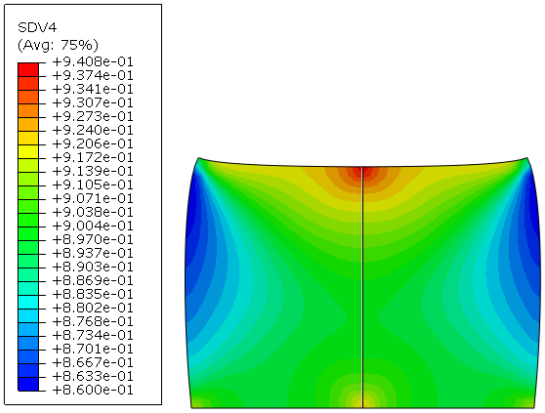

Figure 11. Variation in densification magnitude within the compact at 30% of sintering time.

Figure 11 illustrates the smaller magnitude of densification on the outer vertical edges of the compact. This behavior is consistent based on the shape change.

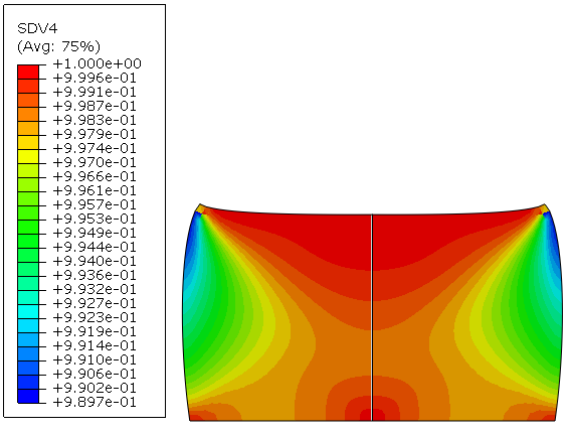

Figure 12. Variation in densification magnitude within the compact at 80% sintering time.

Figure 13 overlays the sintering temperature profile with relative density with leaders to the simulation results presented in figures 10 through 12. It should be noted that a significant portion of the densification occurs over a relatively short time span.

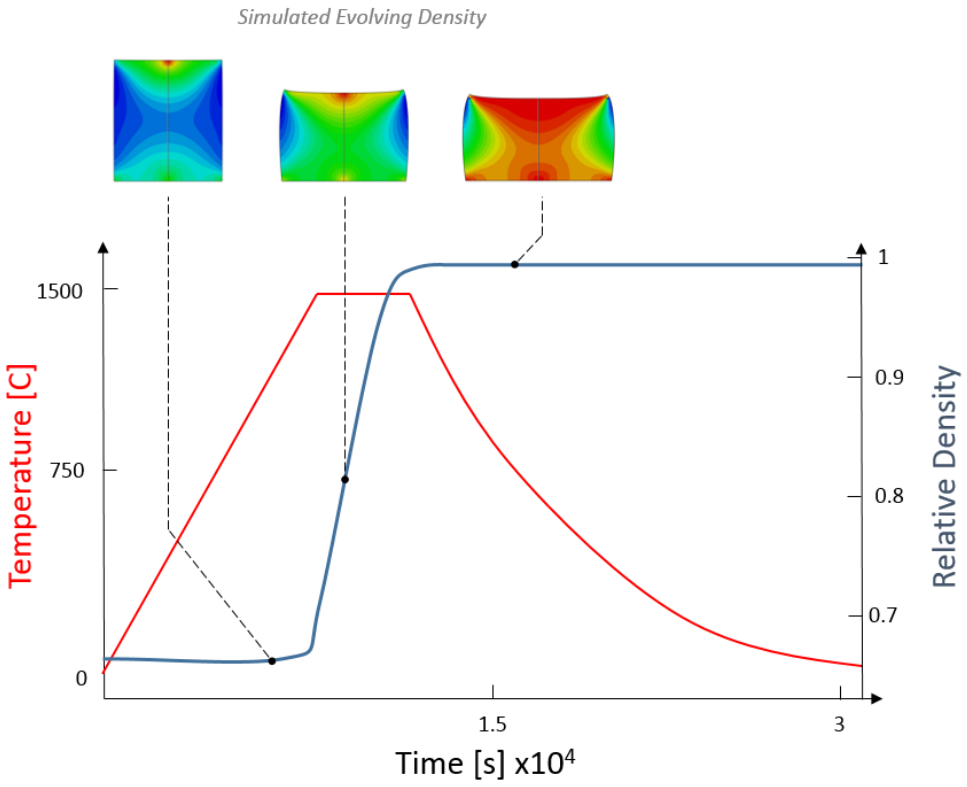

Figure 13. Summary of sintering temperature profile and relative density. Simulated responses denoted on relative density curve.

Figure 14 shows a representation of how the sintering stress results the interaction between the powder particles. Similar to density, the microscale sintering stress defined in the adopted constitutive model is stored in state variable 1 (SDV1).

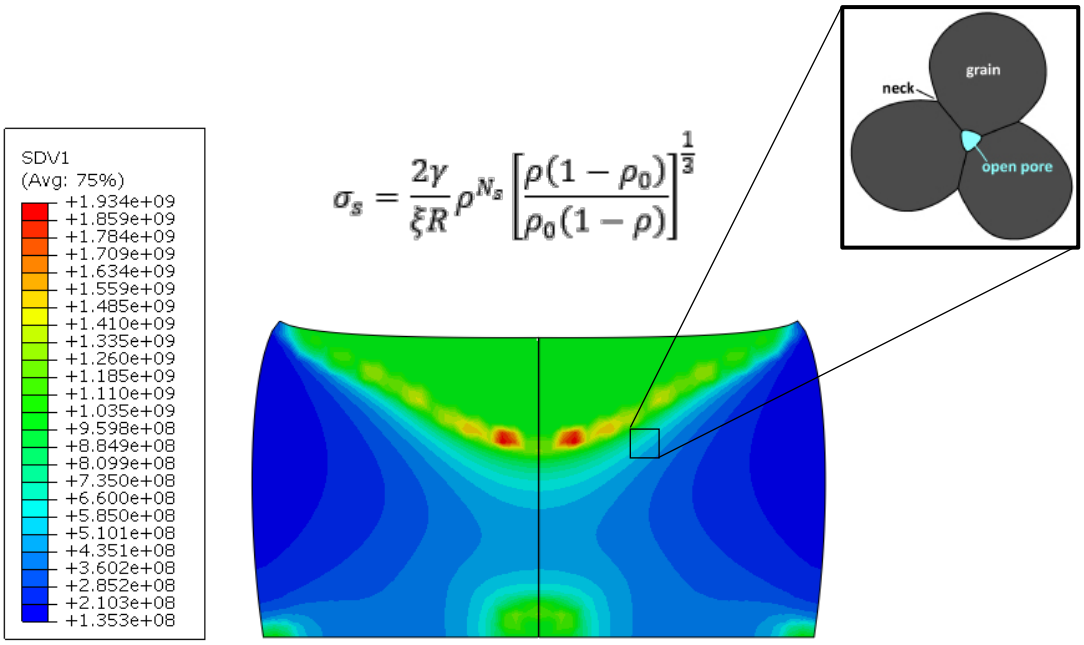

Figure 14. Pattern of microscale sintering stress as defined in equation 14.

3.2 BI-LAYER LAMINATE (2D PLANE STRAIN)

3.2.1 Model process parameters

The next validation case was a bi-layer laminate. This case was also simulated in 2D axisymmetric, initially, to validate the constitutive model. The initial dimensions of the laminate are 40 mm long with a thickness of 0.6 mm for each layer. The initial particle radius was 1 micron. The top layer had an initial green density of 0.61 and the bottom layer had an initial density of 0.64. The two layers were assumed to be bonded together. A representation of one half

of the axisymmetric geometry is shown in figure 15 and the temperature profile is shown in figure 16.

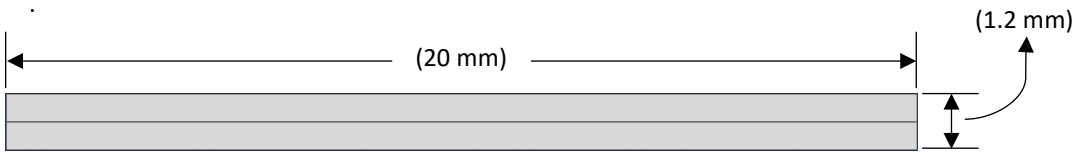

Figure 15. 2-Dimensoinal laminate geometry for validation trial

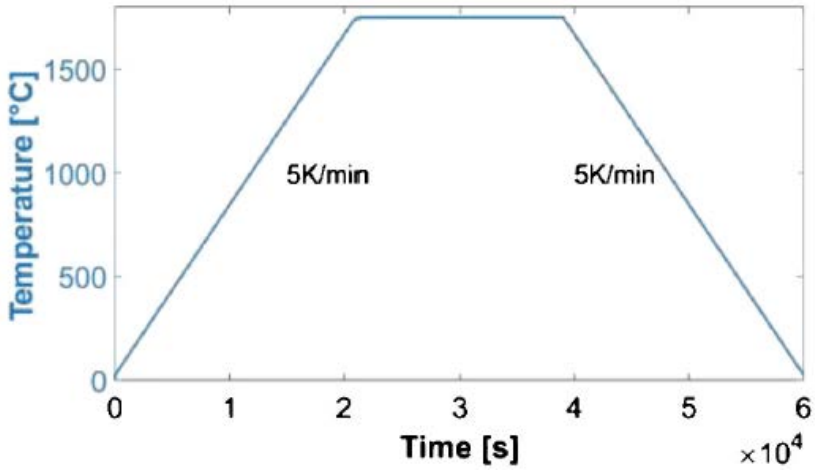

Figure 16. Adopted temperature profile for validation trial

3.2.2 Results

The next set of results describes the geometrical changes in the 2D layered laminate model. This model was expected to curl up on the ends because of the differences in densities between the two layers. Figure 17 shows the comparison between the shape of the laminate before and after sintering. This pattern of deformation was observed and documented by Van et al [6]. The model used assumed plane strain, therefore deformations in the out of plane direction were not resolved. In section 3.3, a 3-dimensional form of this trial model will illustrate the out of plane behavior.

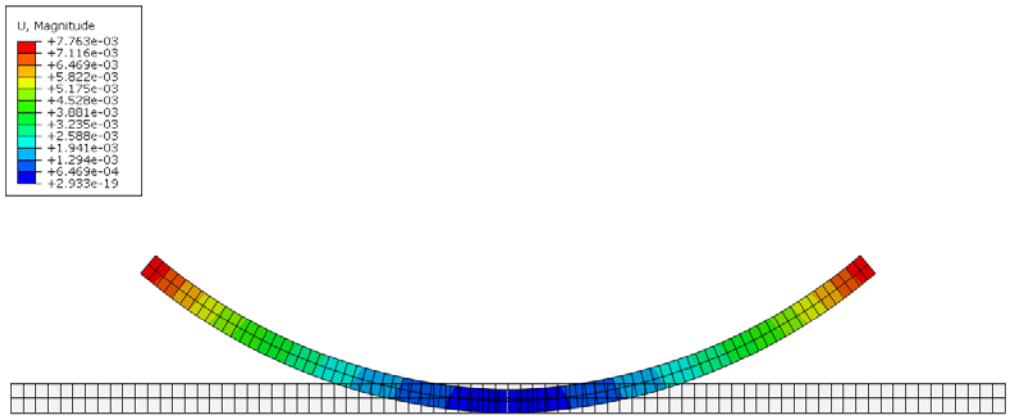

Figure 17. Simulated sintering response of a bi-layered laminate using a plane strain model. Contour overlay illustrates deformation magnitude. Gray overlay represents initial geometry prior to sintering. The "cupping" behavior stems from the distinct difference in density between the two layers.

3.3 BI-LAYER LAMINATE (3-D MODEL)

3.3.1 Model process parameters

Next, the two layer laminate was analyzed in three dimensions. The initial dimensions of the laminate are 40 mm x 15 mm with a thickness of 0.6 mm for each layer. The initial particle radius was 1 micron. The top layer had an initial green density of 0.61 and the bottom layer had an initial density of 0.64. The two layers were assumed to be bonded together. A representation of one quarter of the two axisymmetric geometry is shown in figure 18. The temperature profile is the same as it was for the two dimensional case in section 3.2.

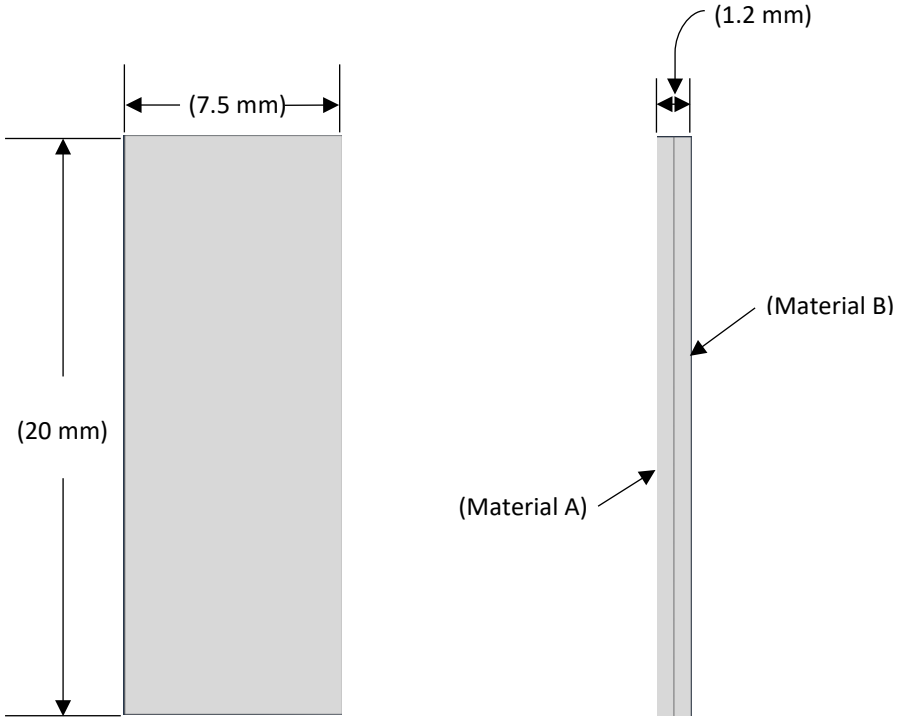

Figure 18. Schematic of 3D laminate geometry for sintering verification trial

3.3.2 Results

The three dimensional case replicates what the 2D laminate case did, but with the distortion in the out of plane direction. The ends were expected to curl up as they did in the two dimensional case, and the corners were expected to curl in. Figure 18 shows that the deformation is what was expected from the literature. The comparison of the simulation to the results found in reference 6 are shown in figures 19 and 20.

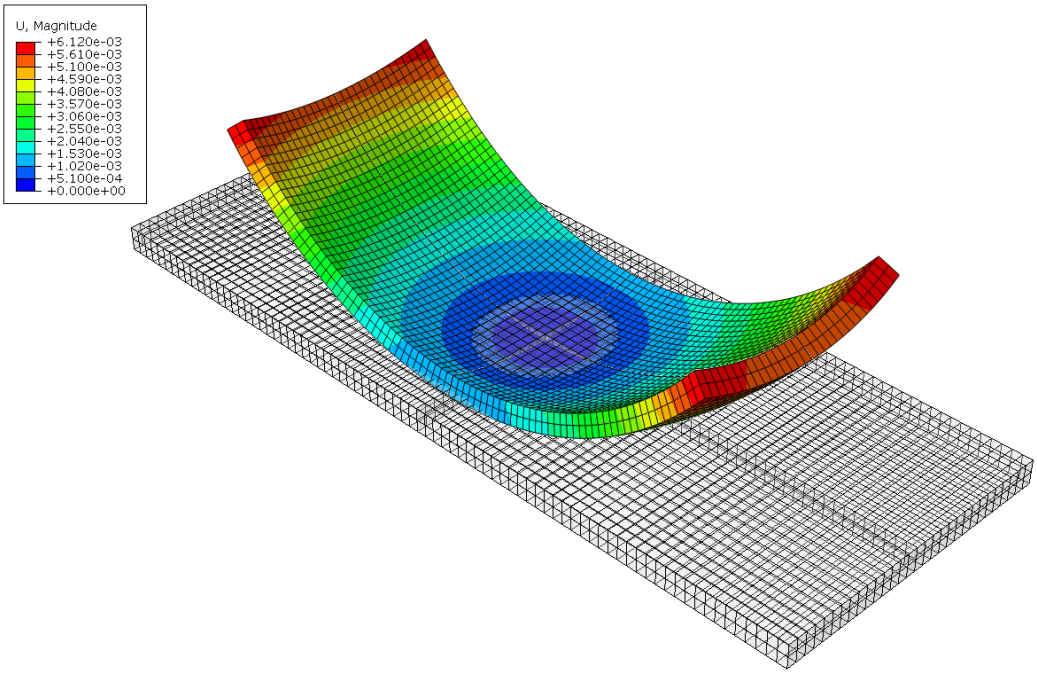

Figure 19. Simulated sintering response of 3 dimensional bi-layered laminate. The contour overlay represents displacement magnitude. The resulting deformation behavior is caused by green density differences between layers

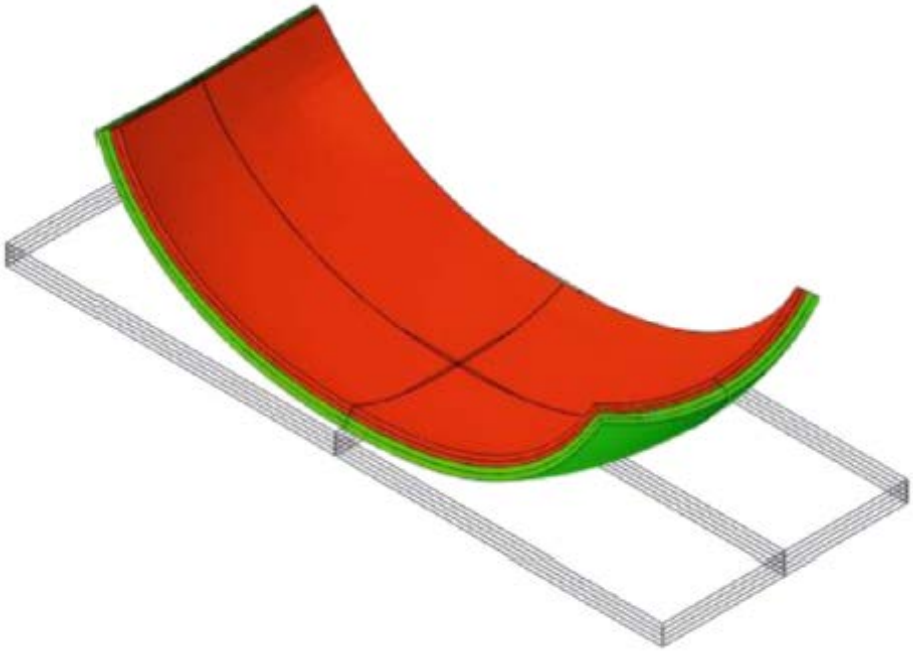

Figure 20. Simulated free sintering response of a bi-layer laminate presented by Van et al [6].

4.0 SIMULATED BASED INVESTIGATION

4.1 TRIAL COMPACT – TRI-LAYER

4.1.1 Model process parameters

When ceramic materials are printed, there is a thin low density layer that is formed in between the printed layers. This layer has different sintering kinetics, and will have an effect on how the two printed layers evolve. This trial aimed at recreating how these three layers interact when sintered. The top and bottom layers had an initial density of 0.3025, and an initial particle radius of 10 microns. The middle layer had an initial density of 0.275 and the same particle size. A representation of a quarter of the axisymmetric geometry is given in figures 21 and 22. The temperature profile is represented in figure 23.

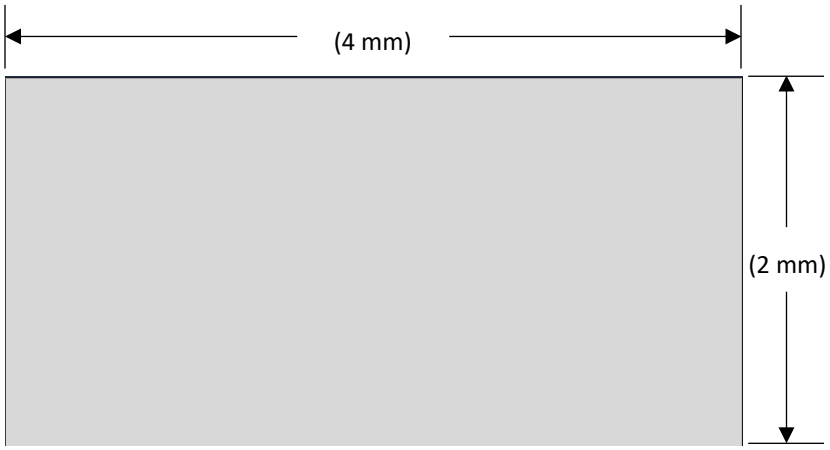

Figure 21. Tri-layer laminate geometry (top view)

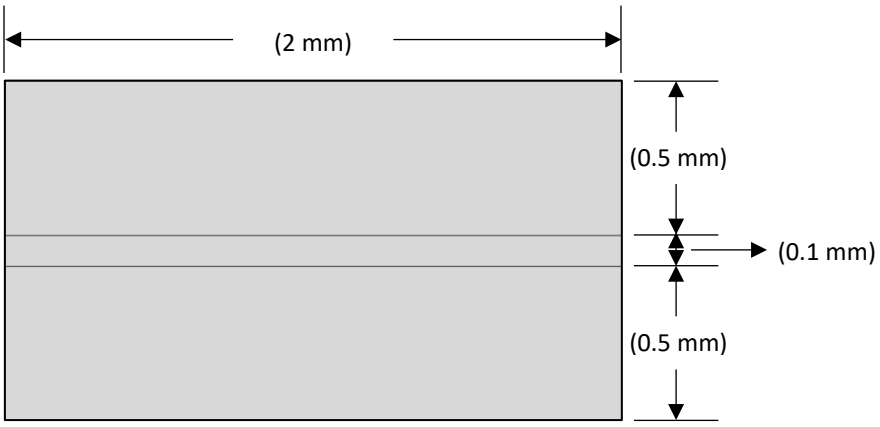

Figure 22. Tri-layer laminate geometry (side view)

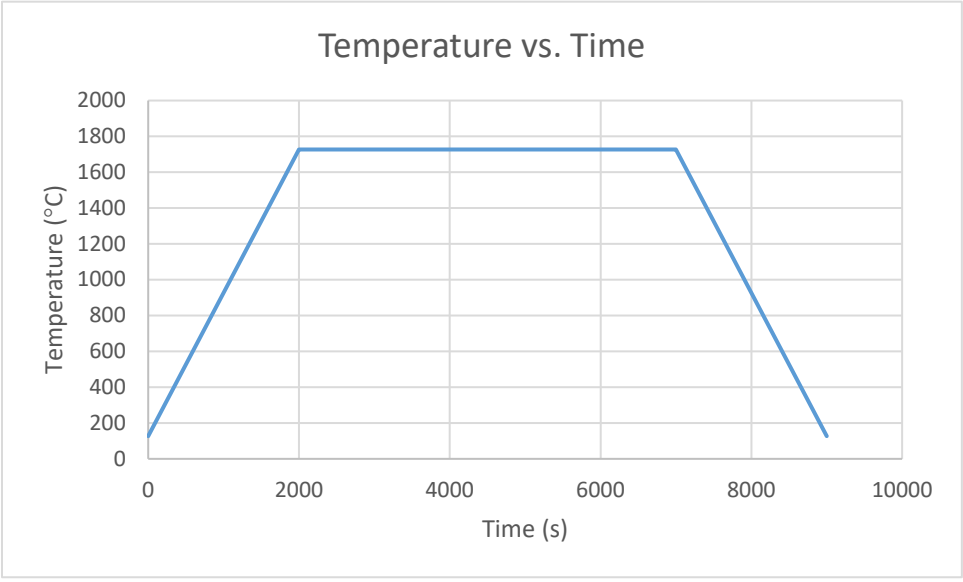

Figure 23. 3-dimensional tri-layer laminate temperature profile for simulation based investigation trial

4.1.2 Results

The tri-layer trial represents the layers that result from printing ceramic parts. In this case, the plot of most concern is the stress. Figure 24 shows the amplification of stress within the thin middle layer.

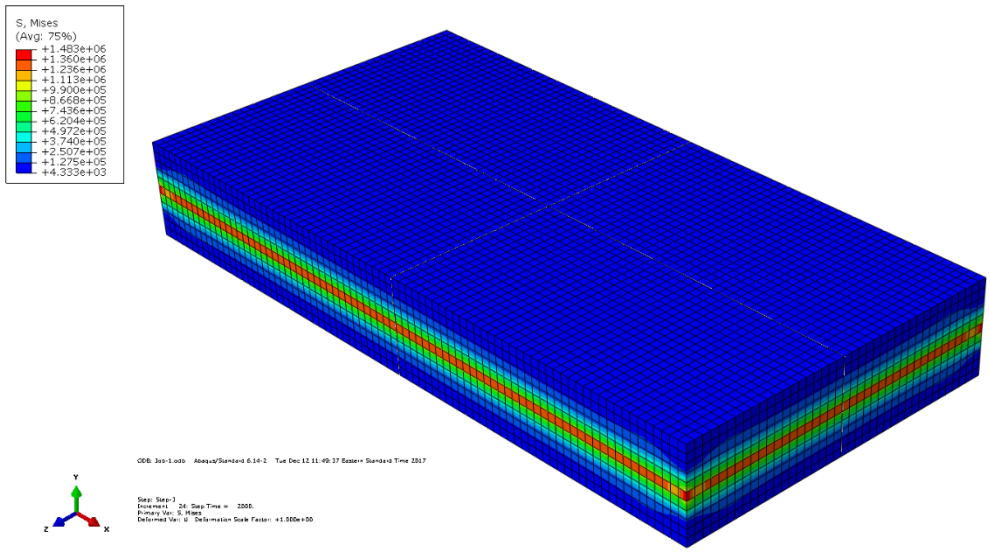

Figure 24. 3D 3 layer laminate stress contour plot for simulation based investigation trial. The stress amplification between the layers is a result of density difference.

5.0 SIMULATED GUIDED GREEN COMPACTS

5.1 ADOPTED PROCESS

Predicting net shape of 3D printed parts is essential to efficiently manufacturing ceramics. The previous method uses a trial and error methodology to sinter several different geometries until a desired shape is achieved. This process is costly and inefficient. The method proposed in this thesis is to use the simulation as a tool to guide the design of the ceramic part geometry. Figure 25 shows a comparison of how the geometry changes using the current process and the modified process proposed in this thesis.

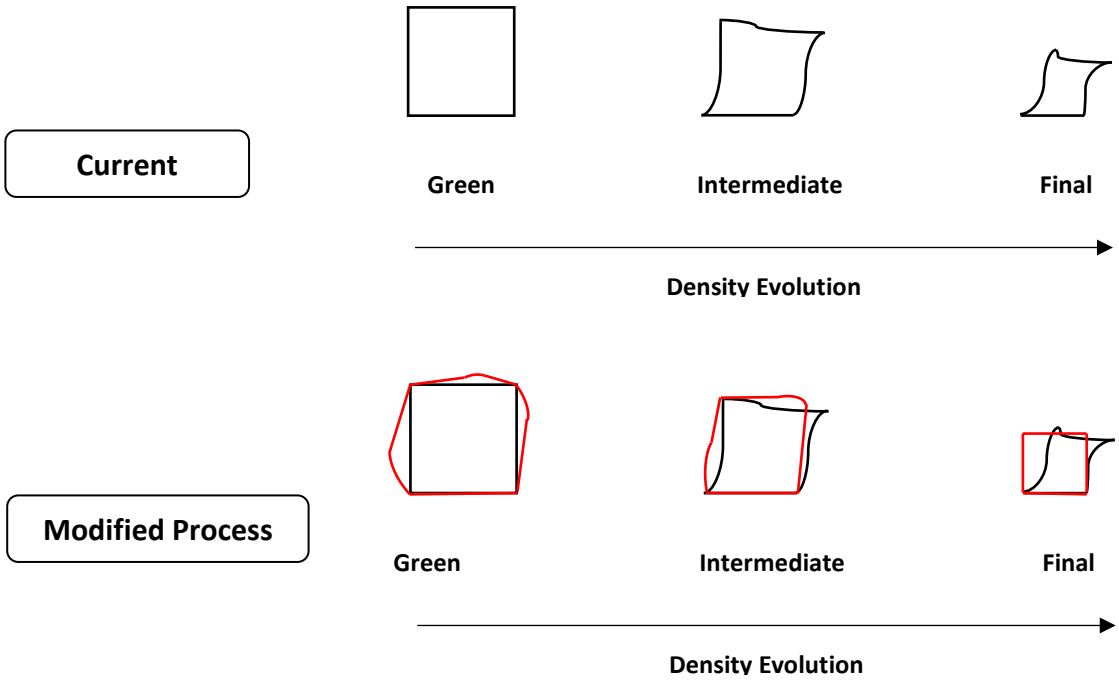

Figure 25. Comparison of compact distortion according to the current process to the modified process. The modified process allows for efficient part design through simulated iterations.

The modified process includes running an initial simulation using the target geometry. Then, the geometry is altered based on an assessment of the distortion after the sintering simulation. This process is repeated until a desired shape is achieved. Figure 26 outlines the steps of using the simulation as a tool to aid in the design process.

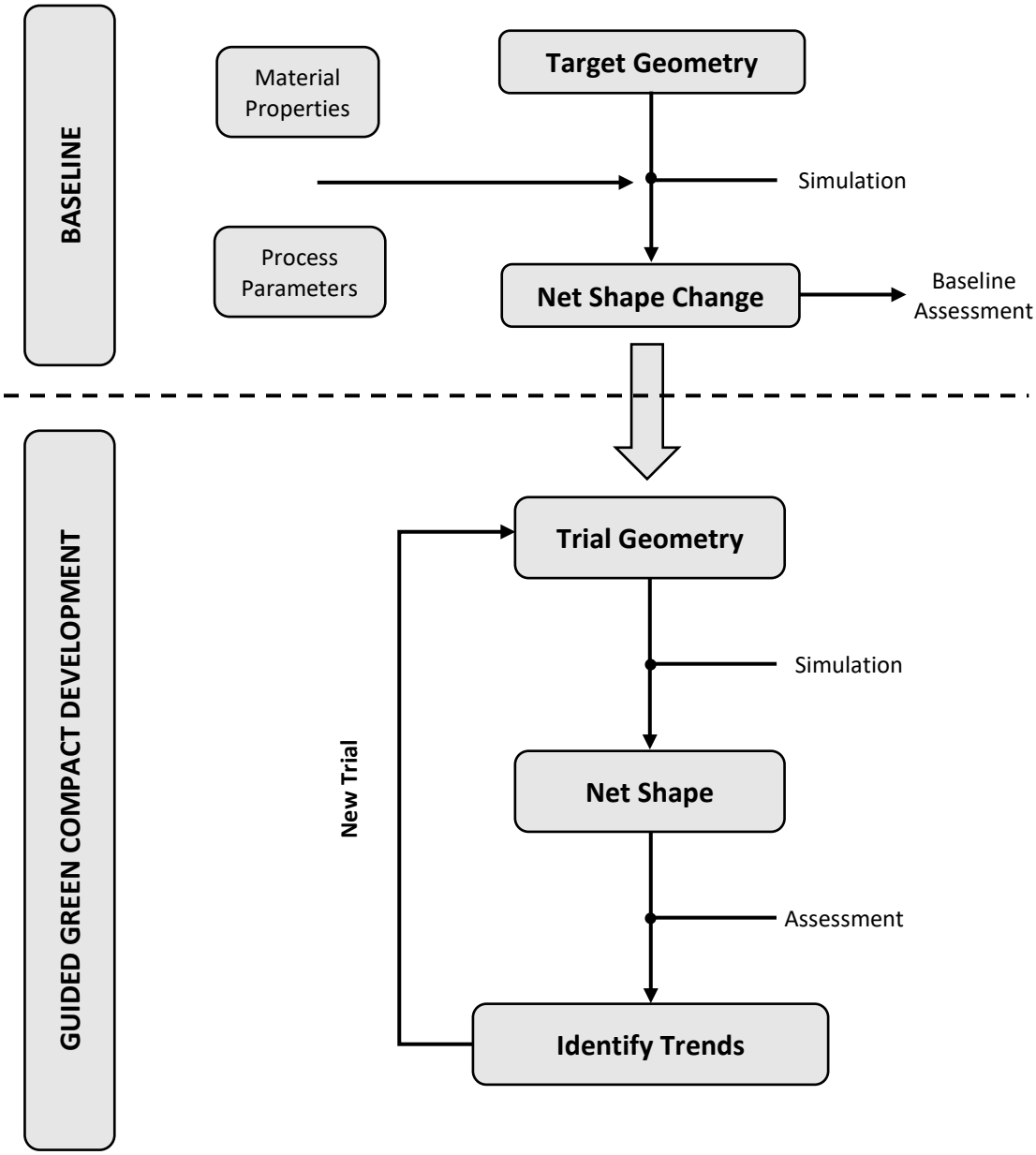

Figure 26. Outline of simulation based process to develop net shape parts after sintering

5.2 TRIAL COMPACT - SQUARE

5.2.1 Model process parameters

The first application of the simulation model is replicating a printed square structure on top of a printed substrate. This would show the dependency of the sintering kinetics on the structure itself and the substrate. The structures started at an initial density of 0.3, while the substrate had an initial density of 0.6. Both the structure and substrate had a starting particle radius of 10 micron. A diagram showing the geometry of the part is given in figure 27. The dimensions of the substrate and temperature profiles are the same for all the trials in chapter 5. The temperature profile is shown in figure 28.

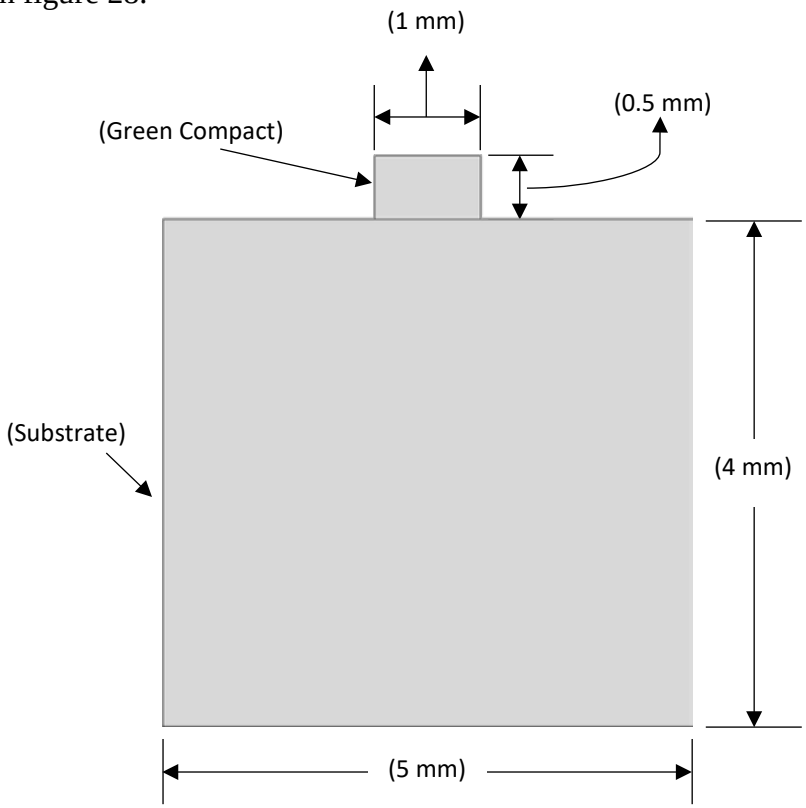

Figure 27. Trial compact - square geometry

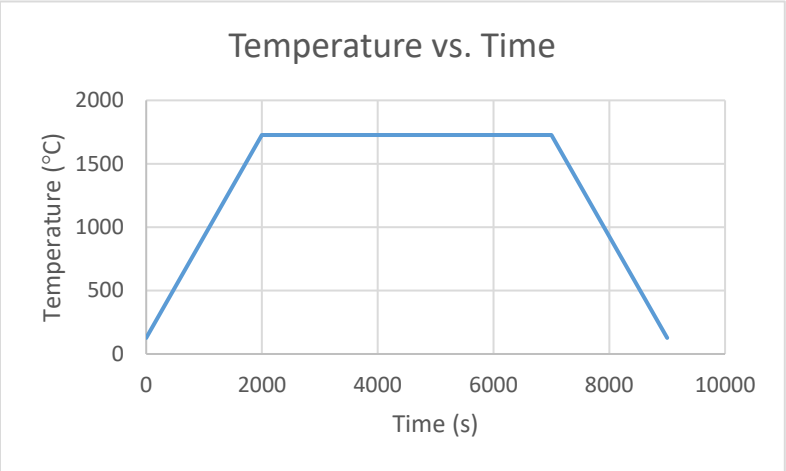

Figure 28. Temperature profile for trial compact simulations

5.2.2 Results

Figure 29 shows the original geometry and the different initial densities. Next, Figures 29 through 32 show the evolution of the density within the part. These plots are captured at multiple increments throughout the simulation. In the model state variable 4 (SDV4) is defined as the density for each time increment.

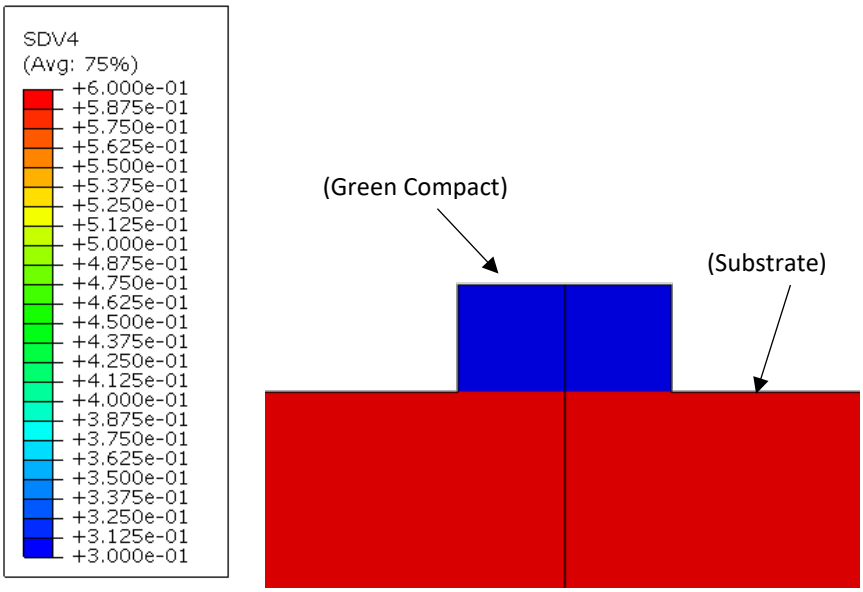

Figure 29. Initial density distribution of square trial compact. The contour overlay illustrates the top structure density of 30 percent with a substrate density of 60 percent.

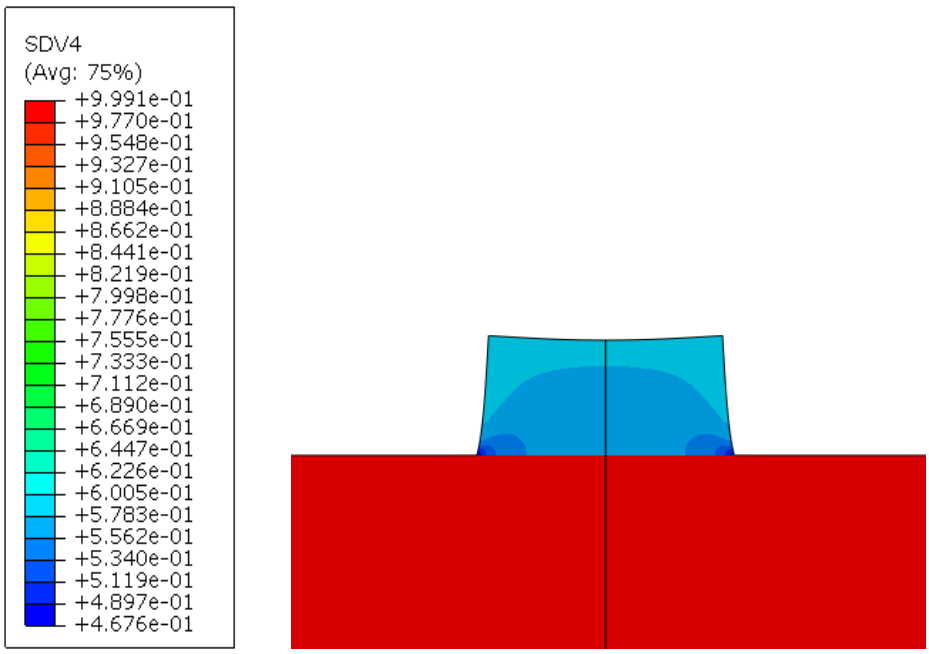

Figure 30. Variation in densification magnitude within compact at 10% sintering time

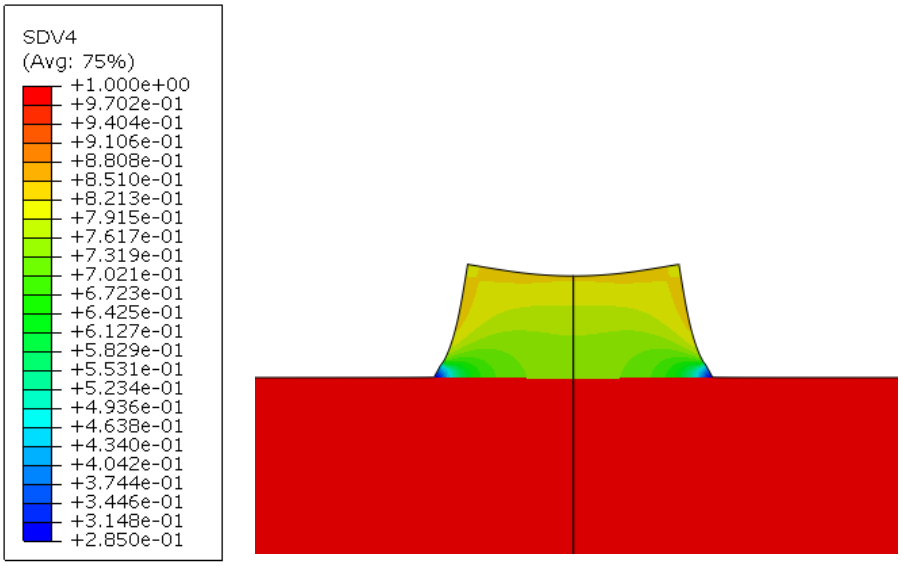

Figure 31. Variation in densification magnitude within compact at 30% sintering time.

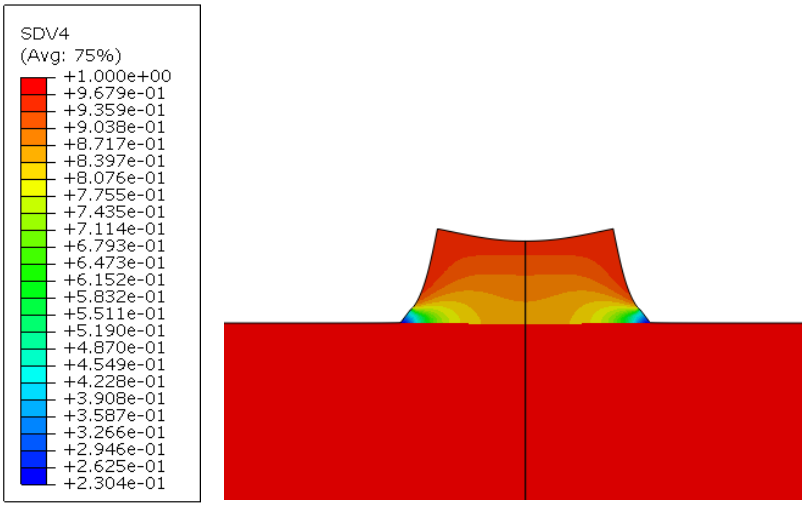

Figure 32. Variation in densification magnitude within compact at 80% sintering time

The top section of the design procedure outlined in figure 26 is represented in figure 33. It can be seen in figure 33 that the nonlinear deformation results in an unwanted geometry profile after sintering. The lower half of figure 26 must be utilized to achieve an acceptable profile.

(Color scale indicates deformation magnitude, red characterizes largest magnitude)

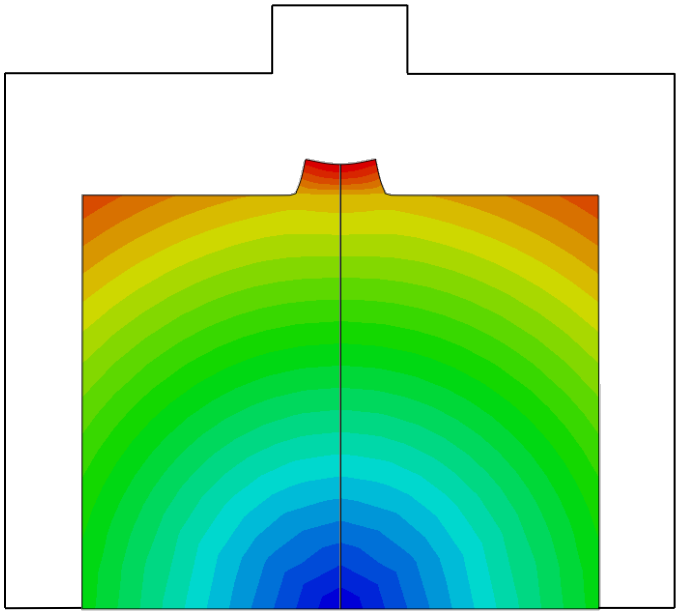

Figure 33. Magnitude of final deformation for pressureless sintering of square geometry. The overlay illustrates the initial compact geometry.

Figure 34 represents the first iteration used achieve the target geometry after sintering. The arrows indicate the modified trial geometries. Figure 34 shows that with the new initial shape, the final geometry is still not satisfactory.

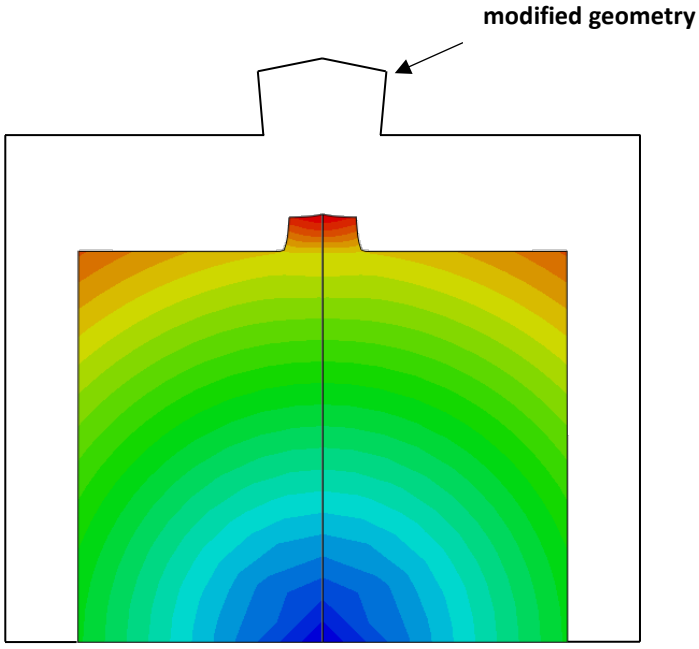

Figure 34. Magnitude of final deformation for pressures sintering of first iteration design. The overlay illustrates the first redesign initial geometry.

Next, figure 35 shows the second iteration of geometry alteration. The resulting shape is closer to the target shape, but more iterations are needed.

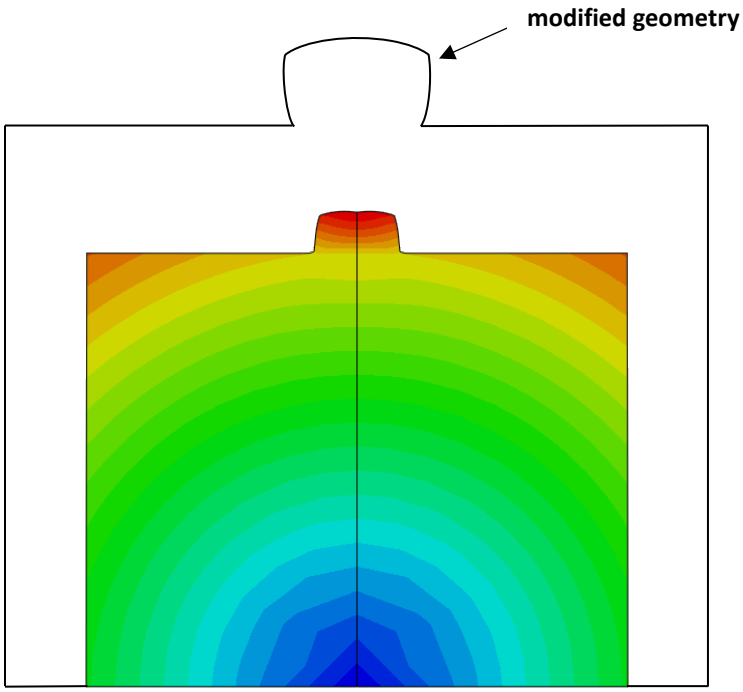

Figure 35. Magnitude of final deformation for pressureless sintering of second iteration design. The overlay represents the second redesign initial geometry.

Through several iterations the initial geometry was altered to result in a square shape after the sintering simulation. The final iteration is shown in figure 36. Observation of net shape change due to densification leads to trends of behavior that can be used to establish potential candidate green compact shapes. Figures 33 through 36 illustrate the process outlined in figure 26. This process includes simulation of the target geometry, then several iterations of design changes in order to achieve the desired resulting shape.

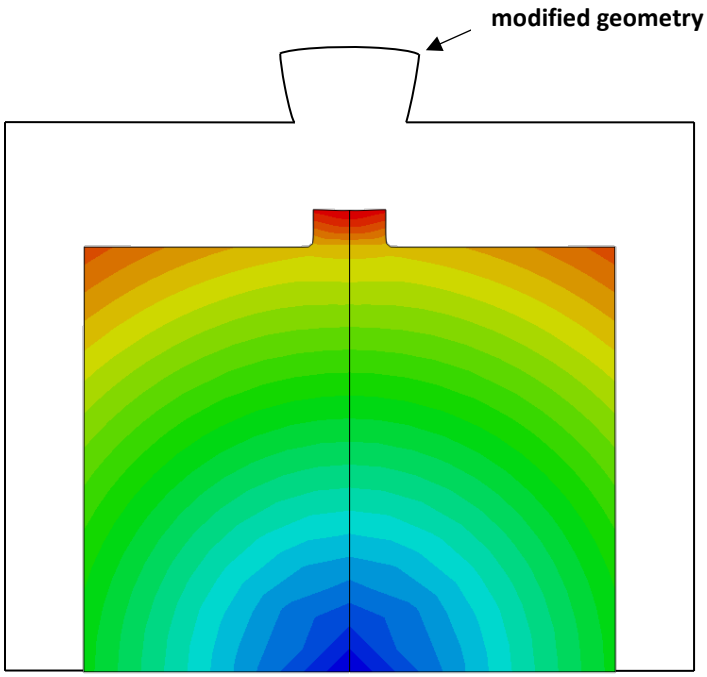

Figure 36. Magnitude of final deformation for pressureless sintering of final design iteration. The overlay represents the final redesign initial geometry.

5.3 TRIAL COMPACT – T SHAPE

5.3.1 Model process parameters

The next application of the simulation model is replicating a printed “T” shaped structure on top of a printed substrate. The structures started at an initial density of 0.3, while the substrate had an initial density of 0.6. Both the structure and substrate had a starting particle radius of 10 micron. A diagram showing the geometry of the part is given in figure 37.

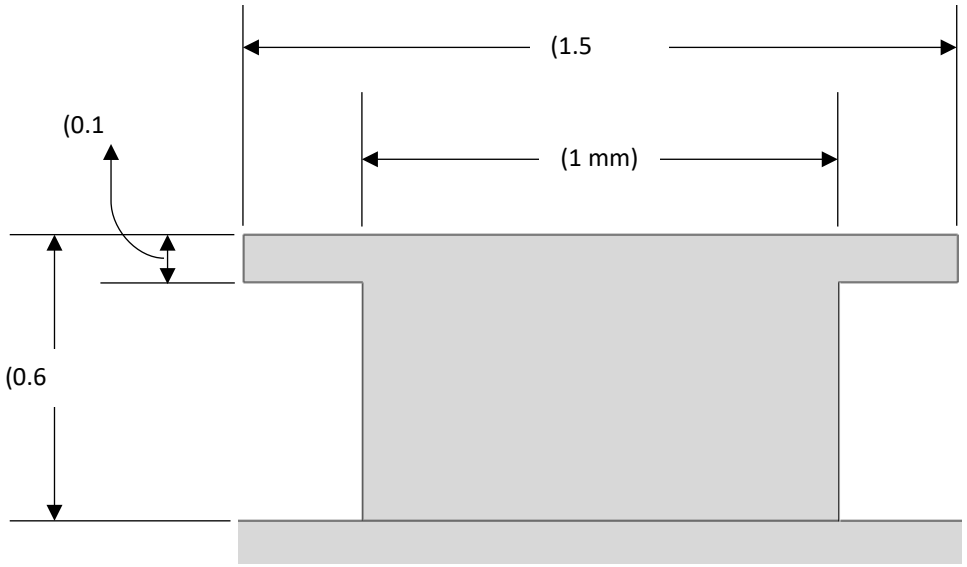

Figure 37. T shape trial compact geometry

5.3.2 Results

Figure 38 shows the displacement of the target geometry after sintering for the "T" shaped trial compact.

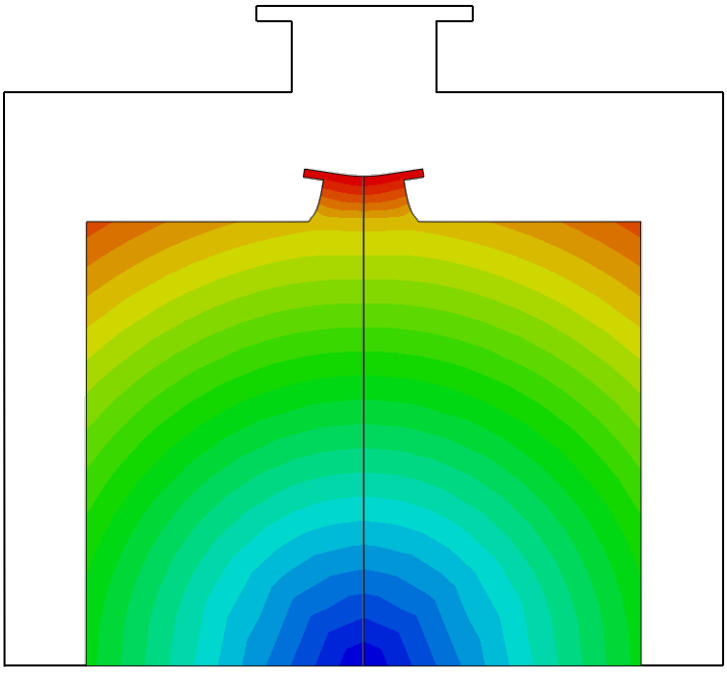

Figure 38. T shape target geometry displacement distribution. The overlay represents the initial geometry.

The same approach was taken, utilizing the process outlined in figure 26. The evolution of the resulting geometry is given in figure 39.

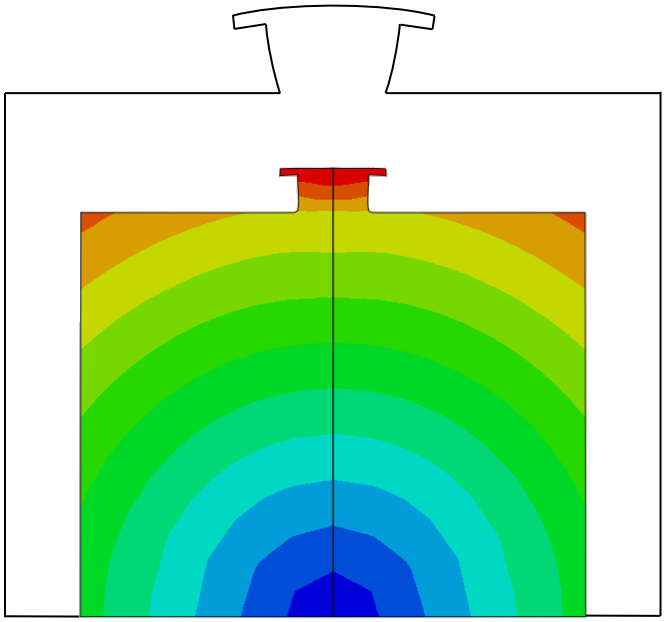

Figure 39. T shape final redesign iteration displacement distribution. The overlay represents the initial geometry

Next, the evolution of density in the T shape trial was analyzed. Figures 40 through 43 show contour plots of the density distribution at increments throughout the simulation. In the model state variable 4 (SDV4) is defined as the density for each time increment.

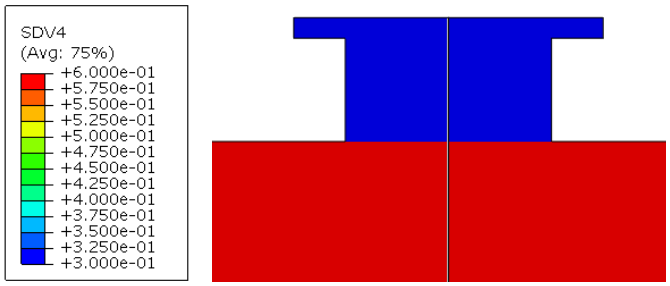

Figure 40. Variation in initial densification of "T" shape compact. The overlay indicates the "T" shape structure has an initial density of 30% while the substrate has an initial density of 60%.

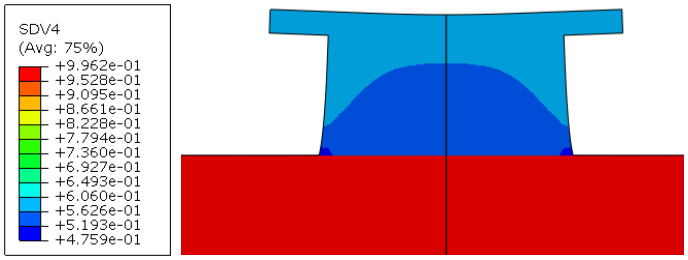

Figure 41. Variation in densification of "T" shape compact at 10% of total sintering time.

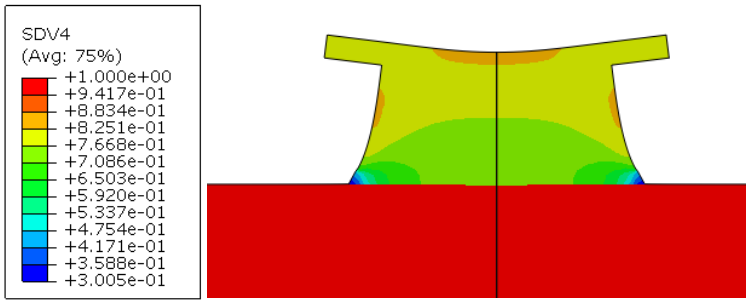

Figure 42. Variation in densification of "T" shape compact at 30% of total sintering time. It is shown that isolated areas are undergoing more rapid densification.

It is seen in figure 42 that densification is occurring more rapidly in particular areas of the compact. Variations in strain drive uneven densification within the compact throughout the sintering process.

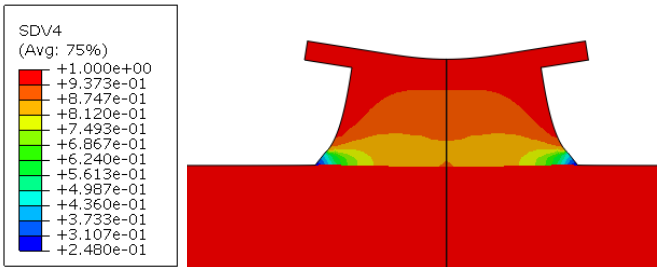

Figure 43. Variation in densification of "T" shape compact at 80% of total sintering time.

5.4 TRIAL COMPACT – H SHAPE

5.4.1 Model process parameters

The last application of the simulation model is replicating a printed “H” structure on top of a printed substrate. This would show the dependency of the sintering kinetics on the structure itself and the substrate. The structures started at an initial density of 0.3, while the substrate had an initial density of 0.6. Both the structure and substrate had a starting particle radius of 10 micron. A diagram showing the geometry of the part is given in figure 44.

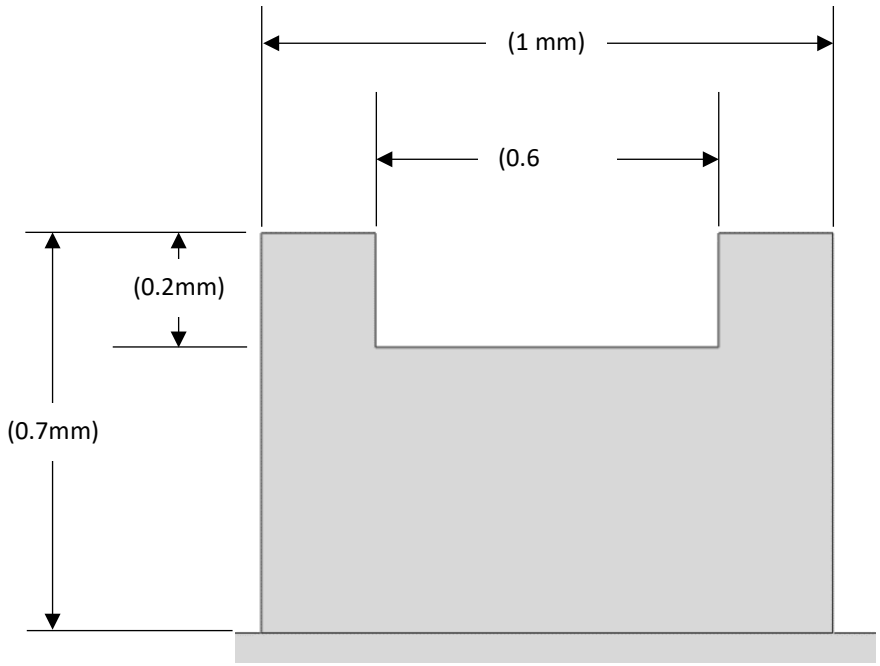

Figure 44. H shape trial compact geometry

5.4.2 Results

Figure 45 shows the displacement of the target geometry after sintering for the “H” shaped trial compact. Redesign of the geometry is needed to develop an acceptable final shape.

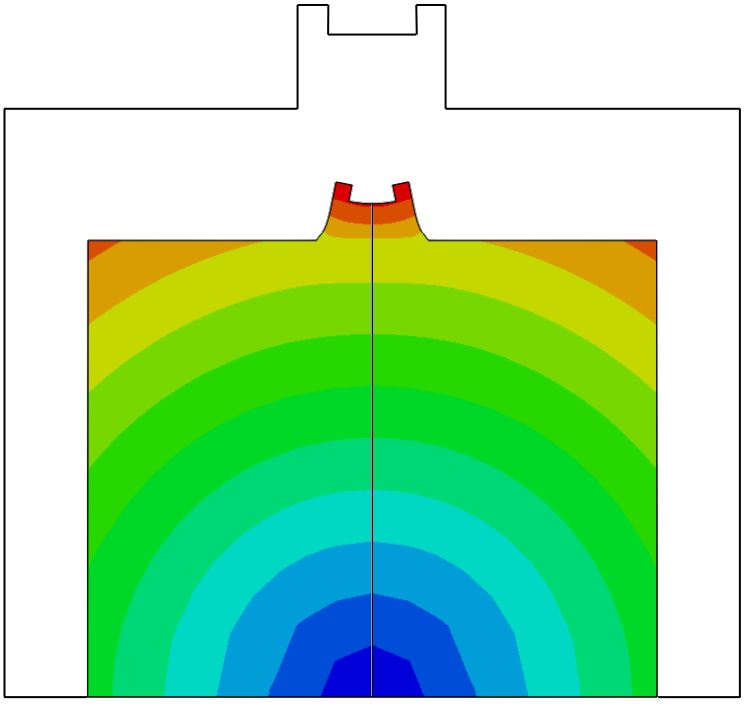

Figure 45. “H” shape target geometry displacement distribution. The overlay indicates the initial shape of the compact before sintering

Several design iterations were used to develop a target net shape that mimicked that of the original geometry. This iterations followed the steps outlined in figure 26. The final geometry evolution is shown in figure 46.

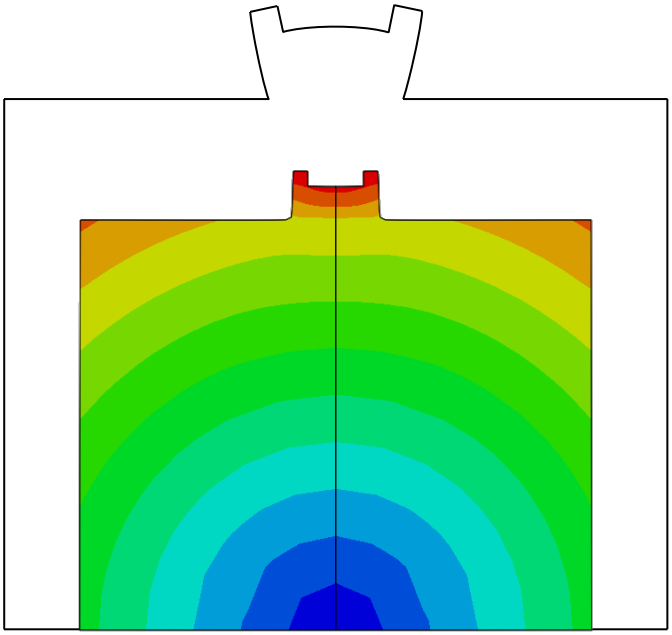

Figure 46. "H" shape final redesign iteration displacement distribution. The overlay shows the geometrical changes necessary to yield the target geometry after sintering.

Next, the evolution of density within the part was analyzed. Figures 47 through 50 are contour plots showing the density distribution at different time increments throughout the simulation. In the model state variable 4 (SDV4) is defined as the density for each time increment.

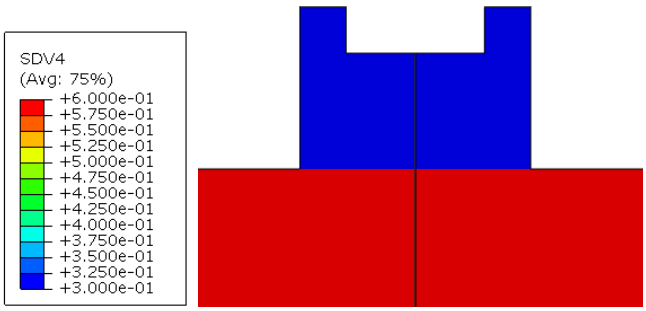

Figure 47. Variation in initial densification of "H" shape compact. The contour plot indicates the top structure has an initial density of 30% while the substrate has an initial density of 60%.

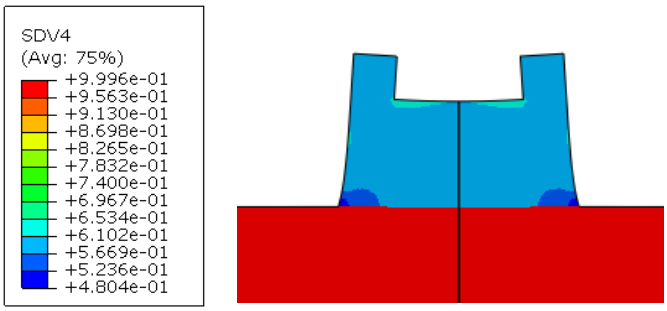

Figure 48. Variation in densification of "H" shape compact at 10% total sintering time.

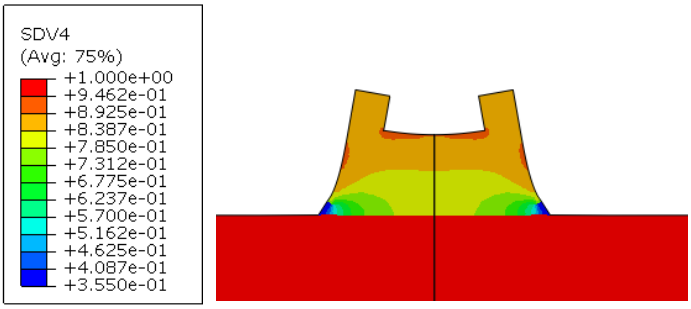

Figure 49. Variation in densification of "H" shape compact at 30% total sintering time.

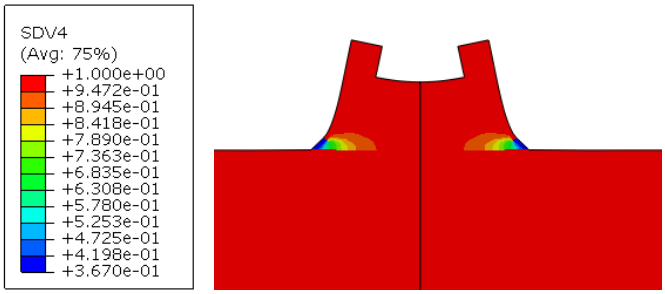

Figure 50. Variation in densification of "H" shape compact at 80% total sintering time.

6.0 DISCUSSION AND FUTURE WORK

The goal of this thesis was to investigate and develop a computational model to predict the shape distortions of sintered aluminum oxide. This was done by developing a constitutive model to predict the mechanical behavior of this material and implement it into FEA software Abaqus. The model was validated by comparing sintering results found in the literature. Once the model was validated, several trials were simulated and analyzed. These trials followed a proposed iterative design process in which a desired shape is achieved after sintering. This process is demonstrated in figure 51.

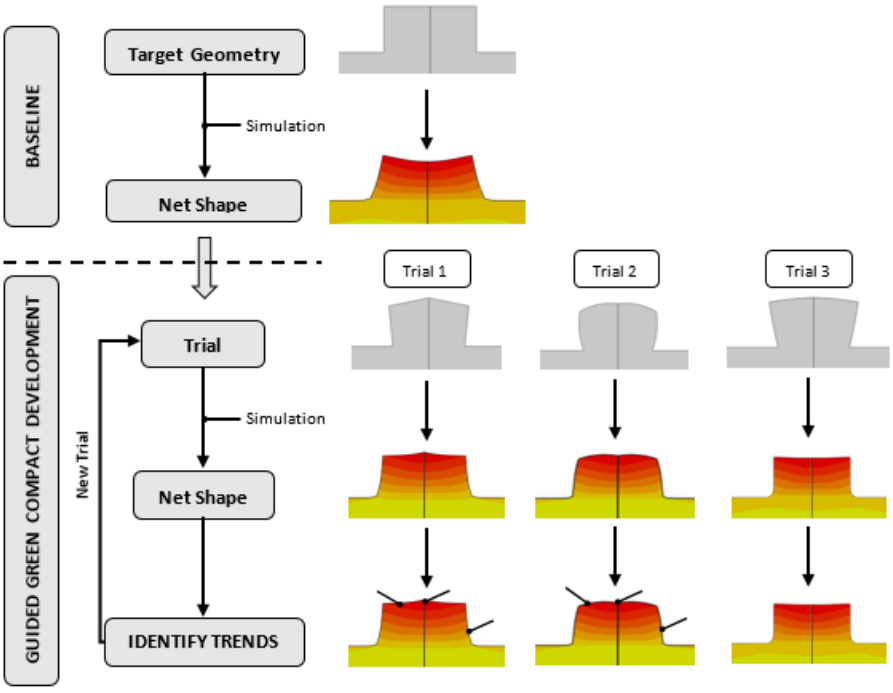

Figure 51. Representation of iterative design process to achieve desired net shape parts after sintering.

A variety of trials were analyzed including multiple printed layers of varying initial densities, and multiple printed structure designs on printed substrates. The accuracy of the moduli (shear and bulk viscosities) were of extreme importance to the simulation. The moduli are what make up the Jacobian matrix. Without accurate formulations for these moduli, the simulation would not converge. Also, the moduli make up the stress increment. Without an accurate stress update, the simulation would not be able to run. The initial shear viscosity seems to be the most sensitive parameter, in this constitutive model. This value is changing exponentially with time, so any variation relating to this parameter has a significant impact in the results.

6.1 FUTURE WORK

This project could be further developed by validating the applied sintering trials. Being able to recreate the simulated results through sintering experiments would add a great deal of validation to this work. Also, many of the parameters in the constitutive model were developed through empirical data. Validation of this parameters could add improvement to the accuracy of the model.

Different sintering simulation trials would be a valuable contribution to research. Sintering layers of different types of ceramics would be a trial of interest. This would require new formulation of the moduli to describe the sintering kinetics. Also, different ceramics may require a different constitutive model. In this case, development of a new UMAT would also be required.

Last, the density distribution evolving throughout the simulation. Being able to capture the evolution of this this parameter is essential to being able to verify changes throughout the

part. The expression for the density is exponential and changes quickly. Figure 52 from reference [8] compares the density evolution in the constitutive model to that of experimental results.

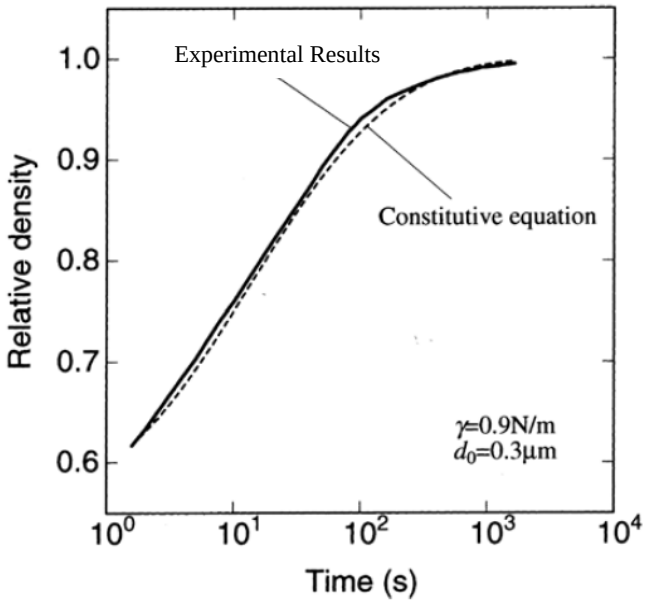

Figure 52. Comparison of density evolution from experimental results to the constitutive equation [8]

As the figure illustrates, the density change occurs quickly compared to the full time of sintering as also seen in figure 13. In order to capture the changes in density, the time increment must be small. This causes long processing time to run the simulation. An improvement could be to code a time increment adjustment into the UMAT. This could be done by recognizing significant changes in density, and setting a flag within the UMAT to trigger a reduction in time step. Although the UMAT approach allows for the definition of a custom constitutive model the time step management associated with the newton-raphson integration method is controlled by Abaqus. This process can be influenced using the parameter PNEWDT within the UMAT to force a decrease in the current time step. By monitoring the changes in density between time steps, the use of this parameter can allow for an appropriate resolution in density changes as

suggested by figure 52. Then, once the density has fully developed, the time increment can be increased again.

APPENDIX A

DERIVATIONS

A.1 JACOBIAN(3D)

$$\Delta\sigma = 4G_p \frac{\Delta\varepsilon}{\Delta t} + \left(2K_p - \frac{4}{3}G_p\right)\frac{\Delta e_{vp}}{\Delta t} I + 2\sigma_s I - 2\sigma_t$$

$$[DSTRAN] = [\Delta\varepsilon] = [\Delta\varepsilon_{11}\,, \Delta\varepsilon_{22}\,, \Delta\varepsilon_{33}\,, \Delta\varepsilon_{12}\,, \Delta\varepsilon_{23}\,, \Delta\varepsilon_{13}]$$

$$\Delta e_{vp} = tr(DSTRAN) = \Delta\varepsilon_{11} + \Delta\varepsilon_{22} + \Delta\varepsilon_{33}$$

$$\frac{\partial\Delta\sigma_{11}}{\partial\Delta\varepsilon_{11}} = \left(\frac{4G_p}{\Delta t}\cdot\frac{\partial(\Delta\varepsilon_{11})}{\partial\Delta\varepsilon_{11}} + \frac{\left(2K_p - \frac{4}{3}G_p\right)}{\Delta t}\cdot\frac{\partial(\Delta\varepsilon_{11}+\Delta\varepsilon_{22}+\Delta\varepsilon_{33})}{\partial\Delta\varepsilon_{11}}\right) = \frac{4G_p}{\Delta t} + \frac{\left(2K_p - \frac{4}{3}G_p\right)}{\Delta t}$$

$$\frac{\partial\Delta\sigma_{11}}{\partial\Delta\varepsilon_{22}} = \left(\frac{4G_p}{\Delta t}\cdot\frac{\partial(\Delta\varepsilon_{11})}{\partial\Delta\varepsilon_{22}} + \frac{\left(2K_p - \frac{4}{3}G_p\right)}{\Delta t}\cdot\frac{\partial(\Delta\varepsilon_{11}+\Delta\varepsilon_{22}+\Delta\varepsilon_{33})}{\partial\Delta\varepsilon_{22}}\right) = \frac{\left(2K_p - \frac{4}{3}G_p\right)}{\Delta t}$$

$$\frac{\partial\Delta\sigma_{11}}{\partial\Delta\varepsilon_{33}} = \left(\frac{4G_p}{\Delta t}\cdot\frac{\partial(\Delta\varepsilon_{11})}{\partial\Delta\varepsilon_{33}} + \frac{\left(2K_p - \frac{4}{3}G_p\right)}{\Delta t}\cdot\frac{\partial(\Delta\varepsilon_{11}+\Delta\varepsilon_{22}+\Delta\varepsilon_{33})}{\partial\Delta\varepsilon_{33}}\right) = \frac{\left(2K_p - \frac{4}{3}G_p\right)}{\Delta t}$$

$$\frac{\partial\Delta\sigma_{11}}{\partial\Delta\varepsilon_{12}} = \left(\frac{4G_p}{\Delta t}\cdot\frac{\partial(\Delta\varepsilon_{11})}{\partial\Delta\varepsilon_{12}} + \frac{\left(2K_p - \frac{4}{3}G_p\right)}{\Delta t}\cdot\frac{\partial(\Delta\varepsilon_{11}+\Delta\varepsilon_{22}+\Delta\varepsilon_{33})}{\partial\Delta\varepsilon_{12}}\right) = 0$$

$$\frac{\partial\Delta\sigma_{11}}{\partial\Delta\varepsilon_{23}} = \left(\frac{4G_p}{\Delta t}\cdot\frac{\partial(\Delta\varepsilon_{11})}{\partial\Delta\varepsilon_{23}} + \frac{\left(2K_p - \frac{4}{3}G_p\right)}{\Delta t}\cdot\frac{\partial(\Delta\varepsilon_{11}+\Delta\varepsilon_{22}+\Delta\varepsilon_{33})}{\partial\Delta\varepsilon_{23}}\right) = 0$$

$$\frac{\partial \Delta\sigma_{11}}{\partial \Delta\varepsilon_{31}} = \left(\frac{4G_p}{\Delta t} \cdot \frac{\partial(\Delta\varepsilon_{11})}{\partial \Delta\varepsilon_{31}} + \frac{\left(2K_p - \frac{4}{3}G_p\right)}{\Delta t} \cdot \frac{\partial(\Delta\varepsilon_{11}+\Delta\varepsilon_{22}+\Delta\varepsilon_{33})}{\partial \Delta\varepsilon_{31}} \right) = 0$$

$$\frac{\partial \Delta\sigma_{22}}{\partial \Delta\varepsilon_{11}} = \left(\frac{4G_p}{\Delta t} \cdot \frac{\partial(\Delta\varepsilon_{22})}{\partial \Delta\varepsilon_{11}} + \frac{\left(2K_p - \frac{4}{3}G_p\right)}{\Delta t} \cdot \frac{\partial(\Delta\varepsilon_{11}+\Delta\varepsilon_{22}+\Delta\varepsilon_{33})}{\partial \Delta\varepsilon_{11}} \right) = \frac{\left(2K_p - \frac{4}{3}G_p\right)}{\Delta t}$$

$$\frac{\partial \Delta\sigma_{22}}{\partial \Delta\varepsilon_{22}} = \left(\frac{4G_p}{\Delta t} \cdot \frac{\partial(\Delta\varepsilon_{22})}{\partial \Delta\varepsilon_{22}} + \frac{\left(2K_p - \frac{4}{3}G_p\right)}{\Delta t} \cdot \frac{\partial(\Delta\varepsilon_{11}+\Delta\varepsilon_{22}+\Delta\varepsilon_{33})}{\partial \Delta\varepsilon_{22}} \right) = \frac{4G_p}{\Delta t} + \frac{\left(2K_p - \frac{4}{3}G_p\right)}{\Delta t}$$

$$\frac{\partial \Delta\sigma_{22}}{\partial \Delta\varepsilon_{33}} = \left(\frac{4G_p}{\Delta t} \cdot \frac{\partial(\Delta\varepsilon_{22})}{\partial \Delta\varepsilon_{33}} + \frac{\left(2K_p - \frac{4}{3}G_p\right)}{\Delta t} \cdot \frac{\partial(\Delta\varepsilon_{11}+\Delta\varepsilon_{22}+\Delta\varepsilon_{33})}{\partial \Delta\varepsilon_{33}} \right) = \frac{\left(2K_p - \frac{4}{3}G_p\right)}{\Delta t}$$

$$\frac{\partial \Delta\sigma_{22}}{\partial \Delta\varepsilon_{12}} = \left(\frac{4G_p}{\Delta t} \cdot \frac{\partial(\Delta\varepsilon_{22})}{\partial \Delta\varepsilon_{12}} + \frac{\left(2K_p - \frac{4}{3}G_p\right)}{\Delta t} \cdot \frac{\partial(\Delta\varepsilon_{11}+\Delta\varepsilon_{22}+\Delta\varepsilon_{33})}{\partial \Delta\varepsilon_{12}} \right) = 0$$

$$\frac{\partial \Delta\sigma_{22}}{\partial \Delta\varepsilon_{23}} = \left(\frac{4G_p}{\Delta t} \cdot \frac{\partial(\Delta\varepsilon_{22})}{\partial \Delta\varepsilon_{23}} + \frac{\left(2K_p - \frac{4}{3}G_p\right)}{\Delta t} \cdot \frac{\partial(\Delta\varepsilon_{11}+\Delta\varepsilon_{22}+\Delta\varepsilon_{33})}{\partial \Delta\varepsilon_{23}} \right) = 0$$

$$\frac{\partial \Delta\sigma_{22}}{\partial \Delta\varepsilon_{31}} = \left(\frac{4G_p}{\Delta t} \cdot \frac{\partial(\Delta\varepsilon_{22})}{\partial \Delta\varepsilon_{31}} + \frac{\left(2K_p - \frac{4}{3}G_p\right)}{\Delta t} \cdot \frac{\partial(\Delta\varepsilon_{11}+\Delta\varepsilon_{22}+\Delta\varepsilon_{33})}{\partial \Delta\varepsilon_{31}} \right) = 0$$

$$\frac{\partial \Delta\sigma_{33}}{\partial \Delta\varepsilon_{11}} = \left(\frac{4G_p}{\Delta t} \cdot \frac{\partial(\Delta\varepsilon_{33})}{\partial \Delta\varepsilon_{11}} + \frac{\left(2K_p - \frac{4}{3}G_p\right)}{\Delta t} \cdot \frac{\partial(\Delta\varepsilon_{11}+\Delta\varepsilon_{22}+\Delta\varepsilon_{33})}{\partial \Delta\varepsilon_{11}} \right) = \frac{\left(2K_p - \frac{4}{3}G_p\right)}{\Delta t}$$

$$\frac{\partial \Delta\sigma_{33}}{\partial \Delta\varepsilon_{22}} = \left(\frac{4G_p}{\Delta t} \cdot \frac{\partial(\Delta\varepsilon_{33})}{\partial \Delta\varepsilon_{22}} + \frac{\left(2K_p - \frac{4}{3}G_p\right)}{\Delta t} \cdot \frac{\partial(\Delta\varepsilon_{11}+\Delta\varepsilon_{22}+\Delta\varepsilon_{33})}{\partial \Delta\varepsilon_{22}} \right) = \frac{\left(2K_p - \frac{4}{3}G_p\right)}{\Delta t}$$

$$\frac{\partial \Delta\sigma_{33}}{\partial \Delta\varepsilon_{33}} = \left(\frac{4G_p}{\Delta t} \cdot \frac{\partial(\Delta\varepsilon_{33})}{\partial \Delta\varepsilon_{33}} + \frac{\left(2K_p - \frac{4}{3}G_p\right)}{\Delta t} \cdot \frac{\partial(\Delta\varepsilon_{11}+\Delta\varepsilon_{22}+\Delta\varepsilon_{33})}{\partial \Delta\varepsilon_{33}} \right) = \frac{4G_p}{\Delta t} + \frac{\left(2K_p - \frac{4}{3}G_p\right)}{\Delta t}$$

$$\frac{\partial \Delta\sigma_{33}}{\partial \Delta\varepsilon_{12}} = \left(\frac{4G_p}{\Delta t} \cdot \frac{\partial(\Delta\varepsilon_{33})}{\partial \Delta\varepsilon_{12}} + \frac{\left(2K_p - \frac{4}{3}G_p\right)}{\Delta t} \cdot \frac{\partial(\Delta\varepsilon_{11}+\Delta\varepsilon_{22}+\Delta\varepsilon_{33})}{\partial \Delta\varepsilon_{12}} \right) = 0$$

$$\frac{\partial \Delta\sigma_{33}}{\partial \Delta\varepsilon_{23}} = \left(\frac{4G_p}{\Delta t} \cdot \frac{\partial(\Delta\varepsilon_{33})}{\partial \Delta\varepsilon_{23}} + \frac{\left(2K_p - \frac{4}{3}G_p\right)}{\Delta t} \cdot \frac{\partial(\Delta\varepsilon_{11}+\Delta\varepsilon_{22}+\Delta\varepsilon_{33})}{\partial \Delta\varepsilon_{23}} \right) = 0$$

$$\frac{\partial \Delta\sigma_{33}}{\partial \Delta\varepsilon_{31}} = \left(\frac{4G_p}{\Delta t} \cdot \frac{\partial(\Delta\varepsilon_{33})}{\partial \Delta\varepsilon_{31}} + \frac{\left(2K_p - \frac{4}{3}G_p\right)}{\Delta t} \cdot \frac{\partial(\Delta\varepsilon_{11}+\Delta\varepsilon_{22}+\Delta\varepsilon_{33})}{\partial \Delta\varepsilon_{31}} \right) = 0$$

$$\frac{\partial \Delta\sigma_{12}}{\partial \Delta\varepsilon_{11}} = \left(\frac{4G_p}{\Delta t} \cdot \frac{\partial(\Delta\varepsilon_{12})}{\partial \Delta\varepsilon_{11}} \right) = 0$$

$$\frac{\partial \Delta\sigma_{12}}{\partial \Delta\varepsilon_{22}} = \left(\frac{4G_p}{\Delta t} \cdot \frac{\partial(\Delta\varepsilon_{12})}{\partial \Delta\varepsilon_{22}} \right) = 0$$

$$\frac{\partial \Delta\sigma_{12}}{\partial \Delta\varepsilon_{33}} = \left(\frac{4G_p}{\Delta t} \cdot \frac{\partial(\Delta\varepsilon_{12})}{\partial \Delta\varepsilon_{33}} \right) = 0$$

$$\frac{\partial \Delta\sigma_{12}}{\partial \Delta\varepsilon_{12}} = \left(\frac{4G_p}{\Delta t} \cdot \frac{\partial(\Delta\varepsilon_{12})}{\partial \Delta\varepsilon_{12}} + \frac{\left(2K_p - \frac{4}{3}G_p\right)}{\Delta t} \cdot \frac{\partial(\Delta\varepsilon_{11}+\Delta\varepsilon_{22}+\Delta\varepsilon_{33})}{\partial \Delta\varepsilon_{12}} \right) = \frac{4G_p}{\Delta t}$$

$$\frac{\partial \Delta\sigma_{12}}{\partial \Delta\varepsilon_{23}} = \left(\frac{4G_p}{\Delta t} \cdot \frac{\partial(\Delta\varepsilon_{12})}{\partial \Delta\varepsilon_{23}} \right) = 0$$

$$\frac{\partial \Delta\sigma_{12}}{\partial \Delta\varepsilon_{31}} = \left(\frac{4G_p}{\Delta t} \cdot \frac{\partial(\Delta\varepsilon_{12})}{\partial \Delta\varepsilon_{31}} \right) = 0$$

$$\frac{\partial \Delta\sigma_{23}}{\partial \Delta\varepsilon_{11}} = \left(\frac{4G_p}{\Delta t} \cdot \frac{\partial(\Delta\varepsilon_{23})}{\partial \Delta\varepsilon_{11}} \right) = 0$$

$$\frac{\partial \Delta\sigma_{23}}{\partial \Delta\varepsilon_{22}} = \left(\frac{4G_p}{\Delta t} \cdot \frac{\partial(\Delta\varepsilon_{23})}{\partial \Delta\varepsilon_{22}} \right) = 0$$

$$\frac{\partial \Delta\sigma_{23}}{\partial \Delta\varepsilon_{33}} = \left(\frac{4G_p}{\Delta t} \cdot \frac{\partial(\Delta\varepsilon_{23})}{\partial \Delta\varepsilon_{33}} \right) = 0$$

$$\frac{\partial \Delta\sigma_{23}}{\partial \Delta\varepsilon_{12}} = \left(\frac{4G_p}{\Delta t} \cdot \frac{\partial(\Delta\varepsilon_{23})}{\partial \Delta\varepsilon_{12}} \right) = 0$$

$$\frac{\partial \Delta\sigma_{23}}{\partial \Delta\varepsilon_{23}} = \left(\frac{4G_p}{\Delta t} \cdot \frac{\partial(\Delta\varepsilon_{23})}{\partial \Delta\varepsilon_{23}} \right) = \frac{4G_p}{\Delta t}$$

$$\frac{\partial \Delta\sigma_{23}}{\partial \Delta\varepsilon_{31}} = \left(\frac{4G_p}{\Delta t} \cdot \frac{\partial(\Delta\varepsilon_{23})}{\partial \Delta\varepsilon_{31}} \right) = 0$$

$$\frac{\partial \Delta\sigma_{31}}{\partial \Delta\varepsilon_{11}} = \left(\frac{4G_p}{\Delta t} \cdot \frac{\partial(\Delta\varepsilon_{31})}{\partial \Delta\varepsilon_{11}} \right) = 0$$

$$\frac{\partial \Delta\sigma_{31}}{\partial \Delta\varepsilon_{22}} = \left(\frac{4G_p}{\Delta t} \cdot \frac{\partial(\Delta\varepsilon_{31})}{\partial \Delta\varepsilon_{22}}\right) = 0$$

$$\frac{\partial \Delta\sigma_{31}}{\partial \Delta\varepsilon_{33}} = \left(\frac{4G_p}{\Delta t} \cdot \frac{\partial(\Delta\varepsilon_{31})}{\partial \Delta\varepsilon_{33}}\right) = 0$$

$$\frac{\partial \Delta\sigma_{31}}{\partial \Delta\varepsilon_{12}} = \left(\frac{4G_p}{\Delta t} \cdot \frac{\partial(\Delta\varepsilon_{31})}{\partial \Delta\varepsilon_{12}}\right) = 0$$

$$\frac{\partial \Delta\sigma_{31}}{\partial \Delta\varepsilon_{23}} = \left(\frac{4G_p}{\Delta t} \cdot \frac{\partial(\Delta\varepsilon_{31})}{\partial \Delta\varepsilon_{23}}\right) = 0$$

$$\frac{\partial \Delta\sigma_{31}}{\partial \Delta\varepsilon_{31}} = \left(\frac{4G_p}{\Delta t} \cdot \frac{\partial(\Delta\varepsilon_{31})}{\partial \Delta\varepsilon_{31}}\right) = \frac{4G_p}{\Delta t}$$

APPENDIX B

UMAT CODE

B.1 LINEAR ELASTIC (3D)

```
      CHARACTER*80 CMNAME
      real test
      real strain_rate(6)
      integer identity(6)
      real new(6)


      DIMENSION STRESS(NTENS),STATEV(NSTATV),
     1 DDSDDE(NTENS,NTENS),DDSDDT(NTENS),DRPLDE(NTENS),
     2 STRAN(NTENS),DSTRAN(NTENS),TIME(2),PREDEF(1),DPRED(1),
     3 PROPS(NPROPS),COORDS(3),DROT(3,3),DFGRD0(3,3),DFGRD1(3,3),
     4 JSTEP(4)


!******ELASTIC USER SUBROUTINE*********

!   Initializing the input parameters and calculating the moduii
      PARAMETER (ONE=1.0D0, TWO=2.0D0)
        E=PROPS(1)
        ANU=PROPS(2)
        ALAMBDA=E/(ONE+ANU)/(ONE-TWO*ANU)
        BLAMBDA=(ONE-ANU)
        CLAMBDA=(ONE-TWO*ANU)

!       Initializing each term of the Jacobian matrix to zero
              DO I=1,NTENS
                  DO J=1,NTENS
                  DDSDDE(I,J)=0.0D0
               ENDDO
            ENDDO

!       Defining the terms in the Jacobian matrix
                     DDSDDE(1,1)=(ALAMBDA*BLAMBDA)
```

```
                    DDSDDE(2,2)=(ALAMBDA*BLAMBDA)
                    DDSDDE(3,3)=(ALAMBDA*BLAMBDA)
                    DDSDDE(4,4)=(ALAMBDA*CLAMBDA)
                    DDSDDE(5,5)=(ALAMBDA*CLAMBDA)
                    DDSDDE(6,6)=(ALAMBDA*CLAMBDA)
                    DDSDDE(1,2)=(ALAMBDA*ANU)
                    DDSDDE(1,3)=(ALAMBDA*ANU)
                    DDSDDE(2,3)=(ALAMBDA*ANU)
                    DDSDDE(2,1)=(ALAMBDA*ANU)
                    DDSDDE(3,1)=(ALAMBDA*ANU)
                    DDSDDE(3,2)=(ALAMBDA*ANU)

!       Updating the incremental stress tensor

         DO I=1,NTENS
               DO J=1,NTENS
               STRESS(I)=STRESS(I)+DDSDDE(I,J)*DSTRAN(J)
               ENDDO
         ENDDO

       RETURN
       END
```

B.2 AXISSYMETRIC CYLINDER/PLANE STRAIN LAMINATE (2D)

```
       SUBROUTINE UMAT(STRESS,STATEV,DDSDDE,SSE,SPD,SCD,
      1 RPL,DDSDDT,DRPLDE,DRPLDT,
      2 STRAN,DSTRAN,TIME,DTIME,TEMP,DTEMP,PREDEF,DPRED,CMNAME,
      3 NDI,NSHR,NTENS,NSTATV,PROPS,NPROPS,COORDS,DROT,PNEWDT,
      4 CELENT,DFGRD0,DFGRD1,NOEL,NPT,LAYER,KSPT,JSTEP,KINC)
!
       INCLUDE 'ABA_PARAM.INC'
!
       CHARACTER*80 CMNAME
       integer, parameter :: dp=selected_real_kind(4,307)

! Initializing the local constants

       real(dp) :: C_s1
       real(dp) :: C_s2
       real(dp) :: n
       real(dp) :: N_s
       real(dp) :: zeta
       real :: gamma
       real :: m
       real(dp) :: beta
       real(dp) :: strain_rate(6)
       real(dp) :: d_3
       real(dp) :: K_p
       real(dp) :: G_p
       real(dp) :: a
       real(dp) :: b
```

```
      real(dp) :: f_s
      real(dp) Sint_S
      real(dp) :: eta
      real(dp) :: RHO



      real identity(4)
      integer :: increment=1

      DIMENSION STRESS(NTENS),STATEV(NSTATV),
     1 DDSDDE(NTENS,NTENS),DDSDDT(NTENS),DRPLDE(NTENS),
     2 STRAN(NTENS),DSTRAN(NTENS),TIME(2),PREDEF(1),DPRED(1),
     3 PROPS(NPROPS),COORDS(3),DROT(3,3),DFGRD0(3,3),DFGRD1(3,3),
     4 JSTEP(4)

!***********The Sintering Subroutine************

! Initialization for the initial density that will be input by the user through the GUI

      PARAMETER(ONE=1.0D0,TWO=2.0D0)
        RHO_0=PROPS(1)
        R=PROPS(2)

! Initializing all of state dependent variables !!!! DON'T FORGET TO ADD DEPVAR IN GUI
!!!!!

        Sint_S=STATEV(1)
        f_s=STATEV(2)
        eta=STATEV(3)
        RHO=STATEV(4)

! Defining all the constants

        C_s1=7.82d15
        C_s2=3.23d4
        n=2.5
        N_s=5.0
        zeta=0.5
        gamma=0.9
        m=1.0/0.37
        beta=4.840d-20
        d_3=(2.0*R)**(3.0)+TEMP*beta

        identity(1)=1.0
        identity(2)=1.0
        identity(3)=1.0
        identity(4)=0



! Define the strain rate tensor matrix

        strain_rate=DSTRAN/DTIME
```

```
! Updating state dependent variables

        RHO=RHO_0*EXP(-STRAN(1)-STRAN(2)-STRAN(3))
        f_s=(1/(2.5*((1.0-RHO)**(1.0/2.0))))

        increment=increment+1.0
        IF (RHO >= 1) THEN
            RHO=0.99999
        END IF

! Calculating the sintering stress

        Sint_S=((2.0*gamma)/(zeta*R))*RHO**(N_s)*((RHO*(1.0-RHO_0))/(RHO_0*(1.0-
RHO)))**(1.0/3.0)


! Calculating the shear viscosity

        eta=(C_s1*TEMP*EXP(C_s2/TEMP)*d_3)

! Defining the shear and bulk moduli

        K_p=3.0*eta*(RHO**(2.0*n-1.0))*(f_s**(2.0))
        G_p=eta*RHO**(2.0*n-1.0)

! Initializing the Jacobian matrix to zero

            DO I=1,NTENS
                DO J=1,NTENS
                    DDSDDE(I,J)=0.0D0
                ENDDO
            ENDDO

! Defining the variables within the Jacobian matrix

        a=2.0*(K_p-(2.0/3.0)*G_p)/DTIME
        b=4.0*G_p/DTIME

! Defining the components of the Jacobian matrix

                DDSDDE(1,1)=a+b
                      DDSDDE(2,2)=a+b
                      DDSDDE(3,3)=a+b
                      DDSDDE(4,4)=b
                      DDSDDE(1,2)=a
                      DDSDDE(1,3)=a
                      DDSDDE(2,3)=a
                      DDSDDE(2,1)=a
                      DDSDDE(3,1)=a
                      DDSDDE(3,2)=a

! Updating the stress tensor

        STRESS(1)=-STRESS(1)+b*DSTRAN(1)+a*(DSTRAN(1)+DSTRAN(2)+DSTRAN(3))+2.0*Sint_S
        STRESS(2)=-STRESS(2)+b*DSTRAN(2)+a*(DSTRAN(1)+DSTRAN(2)+DSTRAN(3))+2.0*Sint_S
        STRESS(3)=-STRESS(3)+b*DSTRAN(3)+a*(DSTRAN(1)+DSTRAN(2)+DSTRAN(3))+2.0*Sint_S
        STRESS(4)=-STRESS(4)+b*DSTRAN(4)
```

```
        STATEV(1)=Sint_S
        STATEV(2)=f_s
        STATEV(3)=eta
        STATEV(4)=RHO

      RETURN
      END
```

B.3 SINTERING SIMULATIONS (3D)

```
      SUBROUTINE UMAT(STRESS,STATEV,DDSDDE,SSE,SPD,SCD,
     1 RPL,DDSDDT,DRPLDE,DRPLDT,
     2 STRAN,DSTRAN,TIME,DTIME,TEMP,DTEMP,PREDEF,DPRED,CMNAME,
     3 NDI,NSHR,NTENS,NSTATV,PROPS,NPROPS,COORDS,DROT,PNEWDT,
     4 CELENT,DFGRD0,DFGRD1,NOEL,NPT,LAYER,KSPT,JSTEP,KINC)
!
      INCLUDE 'ABA_PARAM.INC'
!
      CHARACTER*80 CMNAME
      integer, parameter :: dp=selected_real_kind(4,307)

! Initializing the local constants

      real(dp) :: C_s1
      real(dp) :: C_s2
      real(dp) :: n
      real(dp) :: N_s
      real(dp) :: zeta
      real :: gamma
      real :: m
      real(dp) :: beta
      real(dp) :: strain_rate(6)
      real(dp) :: d_3
      real(dp) :: K_p
      real(dp) :: G_p
      real(dp) :: a
      real(dp) :: b
      real(dp) :: f_s
      real(dp) Sint_S
      real(dp) :: eta
      real(dp) :: RHO

      DIMENSION STRESS(NTENS),STATEV(NSTATV),
     1 DDSDDE(NTENS,NTENS),DDSDDT(NTENS),DRPLDE(NTENS),
     2 STRAN(NTENS),DSTRAN(NTENS),TIME(2),PREDEF(1),DPRED(1),
     3 PROPS(NPROPS),COORDS(3),DROT(3,3),DFGRD0(3,3),DFGRD1(3,3),
     4 JSTEP(4)

!***********The Sintering Subroutine************

! Initialization for the initial density that will be input by the user through the GUI
```

```
      PARAMETER(ONE=1.0D0,TWO=2.0D0)
        RHO_0=PROPS(1)
        R=PROPS(2)


! Initializing all of state dependent variables !!!! DON'T FORGET TO ADD DEPVAR IN GUI
!!!!!

        Sint_S=STATEV(1)
        f_s=STATEV(2)
        eta=STATEV(3)
        RHO=STATEV(4)

! Defining all the constants

        C_s1=7.82*10.0**(15)
        C_s2=3.23d4
        n=2.5
        N_s=5.0
        zeta=0.5
        gamma=0.9
        m=1.0/0.37
        beta=4.840d-20
        d_3=(2.0*R)**(m)+TEMP*beta


! Define the strain rate tensor matrix

        strain_rate=DSTRAN/DTIME

! Defining all the state variables

        RHO=RHO_0*EXP(-STRAN(1)-STRAN(2)-STRAN(3))

        IF (RHO >= 1) THEN
            RHO=0.99999
        END IF

        Sint_S=((2.0*gamma)/(zeta*R))*RHO**(N_s)*((RHO*(1.0-RHO_0))/(RHO_0*(1.0-
RHO)))**(1.0/3.0)

        f_s=(1/(2.5*((1.0-RHO)**(1.0/2.0))))

        eta=(C_s1*TEMP*EXP(C_s2/TEMP)*d_3)

! Defining the shear and bulk modulii

        K_p=3.0*eta*(RHO**(2.0*n-1.0))*(f_s**(2.0))
        G_p=eta*RHO**(2.0*n-1.0)

! Initializing the Jacobian matrix

            DO I=1,NTENS
                DO J=1,NTENS
                    DDSDDE(I,J)=0.0D0
                ENDDO
            ENDDO
```

```
! Defining the variables within the jacobian matrix

        a=2.0*(K_p-(2.0/3.0)*G_p)/DTIME
        b=4.0*G_p/DTIME


! Defining the components of the Jacobian matrix

                DDSDDE(1,1)=a+b
                      DDSDDE(2,2)=a+b
                      DDSDDE(3,3)=a+b
                      DDSDDE(4,4)=b
                      DDSDDE(5,5)=b
                      DDSDDE(6,6)=b
                      DDSDDE(1,2)=a
                      DDSDDE(1,3)=a
                      DDSDDE(2,3)=a
                      DDSDDE(2,1)=a
                      DDSDDE(3,1)=a
                      DDSDDE(3,2)=a

! Updating the components of the stress tensor

        STRESS(1)=-STRESS(1)+b*DSTRAN(1)+a*(DSTRAN(1)+DSTRAN(2)+DSTRAN(3))+2.0*Sint_S
        STRESS(2)=-STRESS(2)+b*DSTRAN(2)+a*(DSTRAN(1)+DSTRAN(2)+DSTRAN(3))+2.0*Sint_S
        STRESS(3)=-STRESS(3)+b*DSTRAN(3)+a*(DSTRAN(1)+DSTRAN(2)+DSTRAN(3))+2.0*Sint_S
        STRESS(4)=-STRESS(4)+b*DSTRAN(4)
        STRESS(5)=-STRESS(5)+b*DSTRAN(5)
        STRESS(6)=-STRESS(6)+b*DSTRAN(6)

        STATEV(1)=Sint_S
        STATEV(2)=f_s
        STATEV(3)=eta
        STATEV(4)=RHO


      RETURN
      END
```

BIBLIOGRAPHY

1. Sōmiya, Shigeyuki. “4.1 Sintering of Ceramics.” *Handbook of Advanced Ceramics.* Amsterdam: Academic, 2003. N. pag. Print.

2. Kraft, Torsten, and Hermann Riedel. “Numerical Simulation of Solid State Sintering; Model and Application.” *Journal of the European Ceramic Society* 24.2 (2004): 345-61. *ScienceDirect.* Web.

3. Carter, C. Barry., et al. “Sintering and Grain Growth.” *Ceramic materials: science and engineering*, Springer Science Business Media, New York, 2007.

4. H. Tanaka, A. Yamamoto, J. Shimoyama, H. Ogino, and K. Kishio, “Strongly connected exsitu MgB 2 polycrystalline bulks fabricated by solid-state self-sintering,” Supercond Sci Technol, 25 [11] 115022 (2012).

5. Olevsky, Eugene A. “Theory of sintering: from discrete to continuum.” Materials Science and Engineering: R: Reports, vol. 23, no. 2, 1998, pp. 41–100., doi:10.1016/s0927796x(98)00009-6.

6. Nguyen Van, Chung & Sistla, Sree. (2016). A comparative study of different sintering models for Al2O3. Journal of the Ceramic Society of Japan. 124. 301-312.10.2109/jcersj2.15257.

7. Kuzmov, A, et al. “Multi-Scale modeling of viscous sintering.” *Modelling and Simulation in Materials Science and Engineering*, vol. 16, no. 3, Nov. 2008, p. 035002., doi:10.1088/0965-0393/16/3/035002.

8. Shinagawa, K. “Micromechanical modelling of viscous sintering and a constitutive equationwith sintering stress.” *Computational Materials Science*, vol. 13, no. 4, 1999, pp. 276–285.,doi:10.1016/s0927-0256(98)00132-3.

9. Reiterer, M. W., et al. “An Arrhenius-Type Viscosity Function to Model Sintering Using the Skorohod-Olevsky Viscous Sintering Model Within a Finite-Element Code.” *Journal of the American Ceramic Society*, vol. 89, no. 6, 2006, pp. 1930–1935., doi:10.1111/j.1551
2916.2006.01041.x.

10. Jiupeng, S. O. N. G. *Experiments, Modelling and Numerical Simulation of the Sintering Process for Metallic or Ceramic Powders*. Diss. PhD-Thesis Shanghai Jiaotong University, China, 2007

11. Molla, Tesfaye Tadesse, Nini Pryds, and Rasmus Bjørk. *Modeling Macroscopic Shape Distortions during Sintering of Multi-layers*. Diss. Department of Energy Conversion and Storage, TechnicalUniversity of Denmark, 2014.

12. Dunne, Fionn, and Nik Petrinic. *Introduction to computational plasticity*. Oxford University Press,

13. R.M. Cannon, W.H. Rhodes, A.H. Heuer, J. Am. Cer. Soc. 63 (1980) 46.

14. Holland, Maria. *The Hitchhiker's Guide to Abaqus*. Aug. 2012, www.bing.com/cr?IG=7D838CBB6EF6495EBA6ED08F2549EC37&CID=2E9B41921D606D761A584AC21C666C20&rd=1&h=iU4Gzi44RZjAgiN5RCC_HC_xQoLbHoXJ-wBUYrw9urY&v=1&r=http%3a%2f%2fweb.stanford.edu%2f%7emholla%2fpdf%2fdocumentation.pdf&p=DevEx,5061.1.